Antibody evasion by the Brazilian P.1 strain of SARS-CoV-2

Wanwisa Dejnirattisai[#,1], Daming Zhou [#,2], Piyada Supasa[#,1], Chang Liu[#,1,3], Alexander J. Mentzer[#,1,4], Helen M. Ginn[5], Yuguang Zhao[2], Helen M.E. Duyvesteyn[2], Aekkachai Tuekprakhon[1], Rungtiwa Nutalai[1], Beibei Wang[1], Guido C. Paesen[2], César López-Camacho[1], Jose Slon-Campos[1], Thomas S. Walter[2], Donal Skelly[4,6,7], Sue Ann Costa Clemens[8], Felipe Gomes Naveca[9], Valdinete Nascimento[9], Fernanda Nascimento[9], Cristiano Fernandes da Costa[10], Paola C. Resende[11], Alex Pauvolid-Correa[11], Marilda M. Siqueira[11], Christina Dold[12,13], Robert Levin[14], Tao Dong[3,15,16], Andrew J. Pollard[12,13], Julian C. Knight[1,4], Derrick Crook[16], Teresa Lambe[17], Elizabeth Clutterbuck[12,13], Sagida Bibi[12,13], Amy Flaxman[17], Mustapha Bittaye[17], Sandra Belij-Rammerstorfer[17], Sarah Gilbert[17], Miles W. Carroll[1,18], Paul Klenerman[4,6,12,19], Eleanor Barnes[4,6,12,19], Susanna J. Dunachie[4,6,20,21], Neil G. Paterson[5], Mark A. Williams[5], David R. Hall[5], Ruben J. G. Hulswit[2], Thomas A. Bowden[2], Elizabeth E. Fry[2], Juthathip Mongkolsapaya[$,1,3,22], Jingshan Ren[$,2], David I. Stuart[$,1,2,3,5,23], Gavin R. Screaton[$,1,3]

1. Wellcome Centre for Human Genetics, Nuffield Department of Medicine, University of Oxford, Oxford, UK.
2. Division of Structural Biology, Nuffield Department of Medicine, University of Oxford, The Wellcome Centre for Human Genetics, Oxford, UK.
3. Chinese Academy of Medical Science (CAMS) Oxford Institute (COI), University of Oxford, Oxford, UK.
4. Oxford University Hospitals NHS Foundation Trust, Oxford, UK.
5. Diamond Light Source Ltd, Harwell Science & Innovation Campus, Didcot, UK.
6. Peter Medawar Building for Pathogen Research, Oxford, UK.
7. Nuffield Department of Clinical Neurosciences, University of Oxford, Oxford, UK
8. Institute of Global Health, University of Siena, Siena, Brazil; Department of Paediatrics, University of Oxford, Oxford, UK.
9. Laboratório de Ecologia de Doenças Transmissíveis na Amazônia, Instituto Leônidas e Maria Deane, Fiocruz, Manaus, Amazonas, Brazil.
10. Fundação de Vigilância em Saúde do Amazonas, Manaus, Amazonas, Brazil
11. Laboratorio de vírus respiratórios- IOC/FIOCRUZ, Rio de Janeiro, Brazil
12.NIHR Oxford Biomedical Research Centre, Oxford, UK.
13. Oxford Vaccine Group, Department of Paediatrics, University of Oxford, Oxford, UK.
14. Worthing Hospital, Worthing, UK.
15. MRC Human Immunology Unit, MRC Weatherall Institute of Molecular Medicine, Radcliffe Department of Medicine, University of Oxford, Oxford, UK.
16. Nuffield Department of Medicine, University of Oxford, Oxford, UK.
17. Jenner Institute, Nuffield Department of Medicine, University of Oxford, Oxford, UK.
18. National Infection Service, Public Health England (PHE), Porton Down, Salisbury, UK..
19. Translational Gastroenterology Unit, University of Oxford, Oxford, UK
20. Centre For Tropical Medicine and Global Health, Nuffield Department of Medicine, University of Oxford, Oxford, UK.
21. Mahidol-Oxford Tropical Medicine Research Unit, Bangkok, Thailand.
Department of Medicine, University of Oxford, Oxford, UK.
22. Siriraj Center of Research Excellence in Dengue & Emerging Pathogens, Dean Office for Research, Faculty of Medicine Siriraj Hospital, Mahidol University, Thailand.
23. Instruct-ERIC, Oxford House, Parkway Court, John Smith Drive, Oxford, UK.

# These authors contributed equally to this work.
$ corresponding authors

Summary

Terminating the SARS-CoV-2 pandemic relies upon pan-global vaccination. Current vaccines elicit neutralizing antibody responses to the virus spike derived from early isolates. However, new strains have emerged with multiple mutations: P.1 from Brazil, B.1.351 from South Africa and B.1.1.7 from the UK (12, 10 and 9 changes in the spike respectively). All have mutations in the ACE2 binding site with P.1 and B.1.351 having a virtually identical triplet: E484K, K417N/T and N501Y, which we show confer similar increased affinity for ACE2. We show that, surprisingly, P.1 is significantly less resistant to naturally acquired or vaccine induced antibody responses than B.1.351 suggesting that changes outside the RBD impact neutralisation. Monoclonal antibody 222 neutralises all three variants despite interacting with two of the ACE2 binding site mutations, we explain this through structural analysis and use the 222 light chain to largely restore neutralization potency to a major class of public antibodies.

Introduction

For more than a year SARS-CoV-2 has caused enormous global dislocation, leading to more than 2.5 million deaths (https://www.worldometers.info/coronavirus Accessed: 2021-03-01) and leaving no country untouched. Successive waves of infection have led to the imposition of draconian lock downs in many countries resulting in severe economic and societal disruption (Donthu and Gustafsson, 2020).

Enormous investment has been made in vaccine development with hundreds of vaccine candidates in different stages of development using an array of different platforms from RNA,

viral vectors, recombinant protein and inactivated (Krammer, 2020). Five vaccines have now been through large scale phase III trials and have demonstrated safety and efficacy (Polack et al., 2020;Voysey et al., 2020;Baden et al., 2020). Four of these, BNT162b2 (Pfizer-BioNTech; mRNA), mRNA-1273 (Moderna; mRNA), ChAdOx1 nCoV-19 (AZD1222) (Oxford-AstraZeneca; chimpanzee adenoviral vectored) and Ad26.COV2-S (Janssen; adenovirus serotype 26 vectored) have received emergency use authorization (EUA) in a variety of countries and are being rolled out at massive scale and NVX-CoV2373 (Novavax; recombinant protein) has also shown impressive efficacy and is likely to achieve EUA in the near future (https://www.medscape.com/viewarticle/944933 Accessed: 2021-03-01). All of these vaccines have been designed to raise antibodies (and T-cells) to spike protein (S) and because of the speed of development they all include S sequences derived from the first reported sequence from Wuhan in January 2020 (Lu et al., 2020).

SARS-CoV-2 like all RNA viruses has an error prone RNA polymerase, and despite some error correction, progressive accrual of mutational changes is inevitable. The massive scale of the pandemic which is largely uncontrolled leads to huge levels of viral replication, increasing the chances that adaptive mutations will occur. There are many possible ways whereby a mutation in SARS-CoV-2 may give the virus a selective advantage, however concentrating on mutation in S, there are two clear possibilities: increased efficiency of transmission and escape from neutralizing antibodies (Volz et al., 2021).

The S protein is a large Type-1 transmembrane glycoprotein which assembles into homo-trimers (Walls et al., 2020), which form most of the outer surface of coronaviruses. S is divided into two portions S1 and S2 which are cleaved by proteolysis. S1 is responsible for target cell engagement, whilst S2 completes membrane fusion allowing the viral RNA access to the host

105 cell cytoplasm where viral replication can begin. S1 contains an N terminal domain (NTD) and
106 receptor binding domain (RBD).
107
108 The RBD interacts with the cellular receptor angiotensin converting enzyme-2 (ACE2) which
109 is expressed on diverse cell types, including cells in the upper and lower respiratory tracts,
110 allowing SARS-CoV-2 to cause respiratory infection. The ACE2 interaction surface is a small
111 25 amino acid patch at the apex of spike, presented to ACE2 when the RBD swings upwards
112 (Hoffmann et al., 2020;Shang et al., 2020) and it is mutations in this region that are causing the
113 most concern. Three multiply mutated viral strains appeared independently at the end of 2020
114 in different regions where they rapidly expanded to become the dominant strains
115 (https://www.cogconsortium.uk/wp-content/uploads/2021/01/Report-2_COG-UK_SARS-
116 CoV-2-Mutations.pdf). It is not clear how these strains acquired so many changes without clear
117 intermediate variants. It has however been speculated, with some evidence, that they may have
118 evolved in immunosuppressed chronically infected patients (Kemp et al., 2021) who support
119 high levels of viral replication for months and may be treated with immune plasma or
120 monoclonal antibodies which may drive selection of variants displaying mutations that evade
121 antibody responses.
122
123 Of most concern are changes in the RBD. P.1 has three: K417T, E484K and N501Y, B.1.351
124 also has three: K417N, E484K and N501Y whereas, B.1.1.7 contains the single N501Y
125 mutation. All of these changes have the potential to modulate ACE2/RBD affinity potentially
126 leading to increased transmissibility, for which there is now good evidence in B.1.1.7. In
127 addition, these mutated residues also have the potential to modulate neutralization of SARS-
128 CoV-2 by naturally or vaccine induced antibody responses.
129

130 In this paper we examine an isolate of P.1 cultured from a throat swab taken from an infected
131 patient in Manaus, Brazil in December 2020 and compare its interactions with serum and
132 antibodies with those of three other viruses, an early isolate, B.1.1.7 and B.1.351. We test the
133 ability of immune sera induced by infection with early strains of SARS-CoV-2 (Dejnirattisai
134 et al., 2021), or by vaccination with the Oxford-AstraZenca or Pfizer-BioNTech vaccines to
135 neutralize P.1 (Supasa et al., 2021;Zhou et al., 2021). We see a reduction in the neutralizing
136 capacity of immune serum to P.1 similar to the reduction seen with B.1.1.7, but not as severe
137 as that seen with B.1.351 (Zhou et al., 2021). We demonstrate an increased affinity of P.1 RBD
138 for ACE2 and investigate the structural basis of this through crystallography. We also study
139 neutralization by a panel of potent monoclonal antibodies which block RBD/ACE2 interaction
140 and provide a crystallographic solution of how one potent antibody, mAb 222, of the panel
141 (Dejnirattisai et al., 2021) which contacts both K417 and N501, is resistant to the 501Y and
142 417T/N mutations found in the P.1/B1.351 strains. We dissect the basis for this via a series of
143 high resolution structures of RDB-Fab complexes and based on this restore neutralization of
144 certain antibodies by swapping the light chain. Finally, we bring together data on P.1, B.1.351
145 and B.1.1.7 and attempt to interpret the different effects these have upon the neutralizing
146 capacity of serum generated to early SARS-CoV-2 strains.
147
148 **Results**
149
150 *The P.1 lineage*
151 P.1 was first reported in December 2020 from Manaus in Amazonas province of Northern
152 Brazil (Faria et al., 2021). A large first wave of infection was seen in Manaus in March-June
153 2020 and by October around 75% of individuals from the region are estimated to have been
154 infected, representing a very high attack rate. A second large wave of infection began in

155 December 2020 leading to further hospitalizations. This second wave corresponded with the
156 rapid emergence of P.1, not seen before December when it was found in 52% of cases, rising
157 to 85% by January 2021 (**Figure S1**).
158
159 P.1 contains multiple changes compared to B.1.1.28 and P.2 which had been previously
160 circulating in Brazil (Faria et al., 2021). Compared to the Wuhan sequence P.1 contains the
161 following mutations: L18F, T20N, P26S, D138Y, R190S in the NTD, K417T, E484K, N501Y
162 in the RBD, D614G and H655Y at the C-terminus of S1 and T1027I, V1176F in S2. The
163 position of the changes seen in P.1 compared with those found in B.1.1.7 and B.1.351 together
164 with a representation on where they occur on the full spike protein and RBD are shown in
165 **Figure 1**. Mutations K417T, E484K, N501Y in the ACE2 interacting surface are of the greatest
166 concern because of their potential to promote escape from the neutralizing antibody response
167 which predominately targets this region (**Figure 1D)** (Dejnirattisai et al., 2021). We searched
168 the COVID-19 genomics UK (COG-UK) (Tatusov et al., 2000) and the global initiative on
169 sharing avian influenza data (GISAID) (https://www.gisaid.org) databases. A small number
170 of sequences including the K417T mutation, inclusive of the P.1 lineage, have been observed
171 in sequencing from Japan, France, Belgium, Italy, the Netherlands and Colombia (**Figure S1**).
172
173 It is noteworthy that P.1, B.1.1.7 and B.1.351 have accrued multiple mutations in the NTD, in
174 B.1.1.7 there are two deletions Δ69-70 and Δ144, in B.1.351 four amino acid changes and the
175 Δ242–244 deletion, while in P.1 there are 6 amino acid changes in the NTD but no deletions.
176 Of note, two of the NTD changes in P.1 introduce N-linked glycosylation sequons T20N (TRT
177 to NRT) and R190S (NLR to NLS, **Figure 1E)**. The NTD, in the absence of these changes,
178 reasonably well populated with glycosylation sites, indeed it has been suggested that a single
179 bare patch surrounded by N-linked glycans glycans attached at N17, N74, N122, and N149

180 defines a 'supersite' limiting where neutralizing antibodies can attach to the NTD (Cerutti et
181 al., 2021). Residue 188 is somewhat occluded whereas residue 20 is highly exposed, is close
182 to the site of attachment of neutralizing antibody 159 (Dejnirattisai et al., 2021) and impinges
183 on the proposed NTD supersite.
184
185 *The effects of RBD mutations on ACE2 affinity.*
186 We have previously measured the affinity of RBD/ACE2 interaction for Wuhan, B.1.1.7
187 (N501Y) and B.1.351 (K417N, E484K, N501Y) RBDs. N501Y increased affinity 7-fold and
188 the combination of 417, 484 and 501 mutations further increased affinity (19-fold compared to
189 Wuhan). Here we have expressed P.1 RBD (K417T, E484K, N501Y). The K_D for the
190 P.1/ACE2 interaction is 4.8 nM with Kon=1.08E5/Ms, Koff=5.18E-4/s (**Figure S2**, Methods),
191 showing that binding to P.1 is essentially indistinguishable from B.1.351 (4.0 nM).
192
193 To better understand RBD-ACE2 interactions we determined the crystal structure of the RBD-
194 ACE2 complex at 3.1 Å resolution (Methods, **Table S1**). As expected the mode of RBD-ACE2
195 engagement is essentially identical for P.1 and the original Wuhan RBD sequence (**Figure**
196 **2A**). The RMS deviation between the 791 Ca positions is 0.4 Å, similar to the experimental
197 error in the coordinates, and the local structure around each of the three mutations is conserved.
198 Nevertheless, calculation of the electrostatic potential of the contact surfaces reveals a marked
199 change, with much greater complementarity for the P.1 RBD consistent with higher affinity.
200 (**Figure 2B,C,D**).
201
202 Residue 417 lies at the back of the RBD neck (our RBD anatomy follows Dejnirattisai et al.,
203 2021) and in the original SARS-CoV-2 is a lysine residue which forms a salt-bridge with D30
204 of ACE2 (**Figure 2E**). The threonine of P.1 RBD no longer forms this interaction and the gap

205 created is open to solvent, so there is no obvious reason why the mutation would increase
206 affinity for ACE2, and this is consistent with directed evolution studies (Zahradník et al., 2021)
207 where this mutation was rarely selected in RBDs with increased affinity for ACE2.
208
209 Residue 484 lies atop the left shoulder of the RBD and neither the original Glu nor the Lys of
210 P1 make significant contact with ACE2, nevertheless the marked change in charge
211 substantially improves the electrostatic complementarity (**Figure 2F,G**), consistent with
212 increased affinity.
213
214 Residue 501 lies on the right shoulder of the RBD and the change from a relatively short Asn
215 sidechain to the large aromatic Tyr allows for favourable ring stacking interactions consistent
216 with increased affinity (**Figure 2H**).
217
218 *Binding of P.1 RBD by potent human monoclonal antibodies*
219 We have previously described a large panel of monoclonal antibodies generated from patients
220 infected with early strains of SARS-CoV-2, before the emergence of B.1.1.7 (Dejnirattisai et
221 al., 2021). From this panel we have selected 20 potent antibodies which have focus reduction
222 neutralization 50% (FRNT50) values <100ng/ml, 19 of these mAbs have an epitope on the
223 RBD and all of these block ACE2/RBD interaction, whilst mAb 159 binds the NTD. We used
224 biolayer interferometry (BLI) to measure the affinity of the RBD-binding antibodies and found
225 that compared to Victoria (SARS-CoV-2/human/AUS/VIC01/2020), an early isolate of SARS-
226 CoV-2, which has a single change S247R in S compared to the Wuhan strain (Seemann et al.,
227 2020; Caly et al., 2020) monoclonal antibody binding was significantly impacted with a
228 number showing complete knock-out of activity (**Figure 2I**). The results with P.1 showed a
229 greater impact compared to B.1.1.7 but similar to B.1.351 (Zhou et al., 2021), this is expected

230 since both contain mutation of the same 3 residues in the RBD, only differing at position 417,
231 K417N in B.1.351 and K417T in P.1. The localization of the impact on binding is shown in
232 **Figure 2J** and reflects direct interaction with mutated residues. Of note is mAb 222 which
233 maintains binding potency across all variants despite adjacency to mutated residues, as
234 discussed below.
235
236 *Neutralization of P.1 by potent human monoclonal antibodies*
237 Using the same set of 20 potent antibodies neutralization was measured by a focus reduction
238 neutralization test (FRNT) and compared with neutralization of Victoria and variants B.1.1.7
239 and B.1.351. Compared to Victoria neutralization by the monoclonal antibodies was
240 significantly impacted by P.1, with 12/20 showing >10-fold reduction in FRNT50 titre and a
241 number showing complete knock out of activity (**Figure 3A Table S2**). The results with P.1
242 showed a greater impact compared to B.1.1.7 but were as expected similar to those with
243 B.1.351 (Zhou et al., 2021). There is good correlation between the negative impact on
244 neutralization and on RBD-affinity (**Figure 2J**).
245
246 *Reduced neutralization of P.1 by monoclonal antibodies being developed for clinical use.*
247 A number of potent neutralizing antibodies are being developed for clinical use either
248 therapeutically of prophylactically (Ku et al., 2021;Baum et al., 2020;Kemp et al., 2021). We
249 performed neutralization assays against P.1 using antibodies S309 Vir (Pinto et al., 2020),
250 AZD8895, AZD1061 and AZ7442 (a combination of AZD8895 and AZD1061) AstraZeneca,
251 REGN10987 and REGN10933 Regeneron, LY-CoV555 and LY-CoV16 Lilly and ADG10,
252 ADG20 and ADG30 from Adagio (**Figure 3B**). The affinity of binding to P.1 RBD was also
253 investigated by BLI for the Regeneron and AstraZeneca antibodies and the results (**Figure 2I**)
254 parallel closely the neutralization results. Neutralization of both Lilly antibodies was severely

255 impacted with LY-CoV16 and LY-CoV555 showing almost complete loss of neutralization of
256 P.1 and B.1.351 while LY-CoV16 also showed marked reduction in neutralization of B.1.1.7.
257 There was also escape from neutralization of P.1 by REGN10933 and a modest reduction in
258 neutralization of P.1 by AZD8895, while AZD1061 and AZD 7442 showed equal
259 neutralization of all SARS-CoV-2 variants. The three Adagio antibodies neutralized all variants
260 with all reaching a plateau at 100% neutralization and interestingly, ADG30 showed a slight
261 increase of neutralization of P.1. S309 Vir was largely unaffected although for several viruses,
262 including P.1, the antibody failed to completely neutralize, conceivably reflecting incomplete
263 glycosylation at N343, since the sugar interaction is key to binding of this antibody N343 (Pinto
264 et al., 2020). The escape from REGN10933 and LY-CoV555 mirrors that of other potent
265 antibodies (including 316 and 384 in our set) which make strong interactions with residues
266 484-486 and are severely compromised by the marked change E484K, whereas LY-CoV016,
267 an IGHV3-53 mAb, is affected by changes at 417 and 501. The abrogation of the Lilly Ly-
268 CoV-16 and LyCoV-555 antibodies reflects the observation of Starr et al. (Starr et al.,
269 2021)(Greaney et al., 2021) that LY-CoV555 is sensitive to mutation at residue 384 and LY-
270 CoV16 is sensitive to changes at 417.
271
272 *Reduced neutralization by an NTD-binding antibody*
273 The neutralization titre of NTD-binding mAb159, was 133-fold reduced on P.1 compared to
274 Victoria with only 64% neutralization at 10μg/ml (**Figures 3A**). Although P.1 does not harbor
275 deletions in the NTD like B.1.1.7 (Δ69−70, Δ144) or B.1.351 (Δ242−244), it is clear that the 6
276 NTD mutations in P.1 (L18F, T20N, P26S, D138Y, R190S) disrupt the epitope for mAb159
277 (**Figure 4A**) (Dejnirattisai et al., 2021;Supasa et al., 2021). It is possible that the failure of this
278 antibody to achieve complete neutralization could be due to partial glycosylation at residue 20,
279 which is some 16 Å from bound Fab 159, however the L18F mutation is even closer and likely

280 to diminish affinity (**Figure 4A**). Since it has been proposed that there is a single supersite for
281 potent NTD binding antibodies we would expect the binding of many of these to be affected
282 (Cerutti et al., 2021).
283
284 *Reduced neutralization by VH3-53 public antibodies*
285 Five of the potent monoclonal antibodies used in this study (150, 158, 175, 222 and 269),
286 belong to the VH3-53 family and a further 2 (out of 5 of this family) belong to the almost
287 identical VH3-66, and the following discussion applies also to these antibodies. The binding
288 sites for these have been described (Dejnirattisai et al., 2021). The large majority of these
289 antibodies attach to the RBD in a very similar fashion. These motifs recur widely, VH3-53 are
290 the most prevalent deposited sequences and structures for SARS-CoV-2 neutralizing
291 antibodies. Their engagement with the RBD is dictated by CDR-H1 and CDR-H2 whilst the
292 CDR-H3 is characteristically short and makes rather few interactions (Yuan et al., 2020; Barnes
293 et al., 2020;Dejnirattisai et al., 2021). We have previously solved the structures of mAbs 150,
294 158 and 269 (**Figure 4B**) which show that whilst there are no contacts with residue 484, there
295 are interactions of CDR-H3 with K417 and CDR-L1 with N501, meaning that binding and
296 neutralization by VH3-53 antibodies would be predicted to be compromised by the N501Y
297 change in variant viruses B.1.1.7, B.1.351 and P.1, whilst the additional change at 417 in P.1
298 (K417T) and B.1.351 (K417N) might be expected to have an additive effect (Dejnirattisai et
299 al., 2021).
300
301 In practice, changes in the light chain and CDR-H3 between members of this family mean that
302 the story is more complex. Thus, neutralization of P.1 by 175 and 158 is severely impacted and
303 neutralization of P.1 by 269 is almost completely lost. However, for 150 P.1 neutralization is

304 less compromised than for B.1.351 (Zhou et al., 2021), whilst for 222 neutralization is
305 completely unaffected by the changes in P.1 and indeed all variants (**Figure 3A**).
306
307 We measured the affinity of 222 for both P.1 (KD = 1.92±0.01 nM) and Wuhan RBD (KD =
308 1.36±0.08 nM) showing no reduction in the strength of interaction despite the changes
309 occurring in the putative binding site for P.1 (**Table S2**).
310
311 To understand how 222 is able to still neutralize P.1 we solved the crystal structures of six
312 ternary complexes of 222 in complex with the RBDs for (i) the original virus, and bearing
313 mutations (ii) K417N; (iii) K417T; (iv) N501Y; the 417, 484 and 501 changes characteristic
314 of B.1.351 (v) and P.1 (vi). All crystals also contained a further Fab, EY6A as a crystallization
315 chaperone (Zhou et al., 2020), were isomorphous and the resolution of the structures ranged
316 from 1.95 to 2.67 Å, **Figure 4C,D**, Methods, **Table S1**. As expected, the structures are highly
317 similar with the binding pose of 222 being essentially identical in all structures (pairwise
318 RMSD in Cα atoms between pairs of structures are ~0.2-0.3 Å for all residues in the RBD and
319 Fv region of mAb 222, **Figure 4D**).
320
321 In the original virus residue 417 makes a weak salt bridge interaction with heavy chain CDR3
322 residue E99. Mutation to either Asn or Thr abolishes this and there is little direct interaction,
323 although there are weak (~3.5 Å) contacts to heavy chain Y52 and light chain Y92 (**Figure**
324 **4E**). However, a buffer molecule/ion rearranges to form bridging interactions and this may
325 mitigate the loss of the salt bridge, in addition the original salt bridge is weak and its
326 contribution to binding may be offset by the loss of entropy in the lysine sidechain. We note
327 that CDR-H3 of 222, at 13 residues is slightly longer than found in the majority of potent VH3-
328 53 antibodies, however this seems unlikely to be responsible for the resilience of 222, rather it

329 seems that there is little binding energy in general from the CDR3-H3, since most of the binding
330 energy contribution of the heavy chain comes from CDR-H1 and CDR-H2 which do not
331 interact with RBD residue 417, meaning that many VH3-53 antibodies are likely to be resilient
332 to the common N/T mutations (**Figure 4B**).
333
334 Residue 501 makes contact with CDR-L1 of mAb 222 (**Figure 4D,F**), however the interaction,
335 with P30 is probably slightly strengthened by the N501Y mutation which provides a stacking
336 interaction with the proline, conferring resilience. This is in contrast to the situation with most
337 other VH3.53 antibodies where direct contacts confer susceptibility to escape by mutation to
338 Tyr (**Figures 2I,J and 3A**) (Supasa et al., 2021;Zhou et al., 2021).
339
340 *The 222 light chain can rescue neutralization by other VH3-53 mAbs*
341 Reasoning that the relative robustness of mAb 222 to common variants (P.1, B.1.1.7 and
342 B.1.351) compared to other VH3-53 antibodies stems from the choice of light chain we
343 modelled the 222LC with the heavy chains of other VH3-53 antibodies to see if they might be
344 compatible **(Figure 4G)**. The result was striking, it appeared that there would likely be no
345 serious steric clashes. This contrasted with the numerous clashes seen when we docked the
346 light chains of other VH3-53 antibodies onto the heavy chain of 222 (**Figure 4G,H**). This
347 suggests that the 222 light chain might be an almost universal light chain for these 3-53
348 antibodies and could confer resilience to P.1, B.1.1.7 and B.1.351 variants. This led us to create
349 chimeric antibodies containing the 222LC combined with the HC of the other VH3-53 mAbs
350 150, 158, 175 and 269. In all cases, chimeric antibodies expressed well and we performed
351 neutralization assays against Victoria, B.1.1.7, B.1.351 and P.1 viruses **(Figure 5)**. For B.1.1.7
352 neutralization of 150HC/222LC, 158HC/222LC and 269HC/222LC was restored to near the
353 level seen on Victoria, whilst 175HC/222LC could not fully neutralize B.1.1.7. For B.1.351

354 and P.1 the activity of mAbs 150 and 158 was restored in chimeras containing the 222LC, with
355 the 150HC/222LC showing 50-fold greater potency against B.1.351 (7ng vs 350 ng/ml) and
356 13-fold greater potency against P.1 (3ng vs 40 ng/ml) than native 150. With an FRNT50 of
357 3ng/ml 150HC/222LC was the most potent antibody tested against P.1.
358
359 *Neutralization of P.1 by convalescent plasma*
360 We collected convalescent plasma samples from a cohort of volunteers who had suffered from
361 SARS-CoV-2 infection evidenced by a positive diagnostic PCR. Samples were collected
362 during the convalescent phase, 4-9 weeks following infection, all samples were taken during
363 the first wave of infection in the UK, prior June 2020 and well before the emergence of the
364 B.1.1.7 variant. We have also collected plasma from volunteers recently infected with B.1.1.7
365 as demonstrated by viral sequencing or S gene drop out from the diagnostic PCR (Dejnirattisai
366 et al., 2021;Supasa et al., 2021).
367
368 Neutralization of P.1 was assessed by FRNT on 34 convalescent samples **(Figure 6A Table**
369 **S3A)**. P.1 neutralization curves are displayed alongside neutralization curves for Victoria,
370 together with B.1.1.7 and B.1.351. P.1 geometric mean neutralization titres were reduced 3.1-
371 fold compared to Victoria ($p< 0.0001$). This reduction was similar to B.1.1.7 (2.9-fold) and
372 considerably less than B.1.351 (13.3-fold) **(Figure 6C)**. When using plasma from individuals
373 infected with B.1.1.7 we saw only modest (1.8-fold $p=0.0039$) reductions in neutralization
374 comparing P.1 with Victoria **(Figure 6B and D Table S3B)**.
375
376 *Neutralization of P.1 by vaccine serum*
377 We next performed neutralization assays using serum collected from individuals who had
378 received either the BNT162b2 Pfizer-BioNTech or ChAdOx1 nCoV-19 Oxford-AstraZeneca

379 vaccine **Figure 7** (Supasa et al., 2021;Zhou et al., 2021). For the Pfizer BioNTech vaccine
380 serum was collected 4-14 days following the second dose of vaccine administered three weeks
381 after the first dose (n=25). For the Oxford-AstraZeneca vaccine serum was taken 14 or 28 days
382 following the second dose which was administered 8-14 weeks following the first dose (N=25).
383 Geometric mean neutralization titres against P.1 were reduced 2.6-fold ($p<0.0001$) relative to
384 the Victoria virus for the Pfizer-BioNTech vaccine serum **Figure 7A,C** and 2.9-fold
385 ($P<0.0001$) for the Oxford-AstraZeneca vaccine **Figure 7B,D Table S4.**
386
387 Neutralization titres against P.1 were similar to those against B.1.1.7 and only a minority of
388 samples failed to reach 100% neutralization at 1:20 dilution of serum, considerably better than
389 neutralization of B.1.351, where titres were reduced 7.6-fold and 9-fold for the BNT162b2
390 Pfizer and ChAdOx1 nCoV-19 AstraZeneca vaccines respectively.
391
392 **Discussion**
393
394 Large scale viral sequencing programmes have uncovered a spectrum of mutations containing
395 changes at many locations in the SARS-CoV-2 genome in correspondence with the concept of
396 viral quasispecies (Domingo and Perales, 2019). Mutations in S are of particular concern as S,
397 through the RBD, directs cellular tropism and in addition is the target for the neutralizing
398 antibody response. Mutations in S could therefore enhance viral fitness by increasing affinity
399 to ACE2 or provide escape from the antibody response induced by natural infection or
400 vaccination.
401
402 P.1 contains 12 individual changes spread throughout S with three changes in the RBD. In this
403 paper we demonstrate an increase in affinity of interaction for P.1 RBD with ACE2 to an

404 equivalent degree as that observed for B.1.351 with binding somewhat tighter than for B.1.1.7.
405 It seems conceivable that this increase in receptor affinity may drive increased virus
406 transmissibility, allowing the three variants to become dominant strains in the regions where
407 they emerged (Zhou et al., 2021;Supasa et al., 2021).
408
409 The ACE2 interacting surface of RBD is a small 25 amino acid patch at the apex of S and is
410 under extreme selection pressure as it not only mediates interaction with the cellular receptor
411 but is also the site of binding for a major class of neutralizing antibodies that block the
412 interaction of ACE2 with the RBD (Zost et al., 2020;Kreye et al., 2020;Wu et al., 2020;Yuan
413 et al., 2020). (Dejnirattisai et al., 2021). Recently, two elegant unbiased approaches have been
414 used to assess the influence of mutation on the ACE2/RBD binding affinity or the ability of
415 RBD mutations to evade the polyclonal antibody response. Firstly, a yeast display approach
416 was used to generate RBD mutants with enhanced ACE2 binding. Amongst a number of
417 mutations selected were the very same positions found in the recent variants of concern, namely
418 E484K and N501Y, and less frequently changes at residue 417 were also observed (Zahradník
419 et al., 2021). Multiple rounds of selection led to the emergence of mutant RBDs with 600-fold
420 higher affinity to ACE2, in the low picomolar range. In a second approach, polyclonal anti-
421 SARS-CoV-2 serum was used to select mutant RBD from a yeast display library which showed
422 reduced antibody binding (Greaney et al., 2021). This approach led to the identification of a
423 number of potential antibody escape mutants, amongst them E484 which is likely responsible
424 for a proportion of the escape from antibody neutralization we describe for P.1.
425
426 What is driving the emergence of the new strains is difficult to determine, the emergence of
427 B.1.1.7 occurred on the background of relatively low population immunity and may have been
428 primarily driven by increased transmissibility. The emergence of B.1.351 occurred on the

429 background of around 30% seropositivity in South Africa and P.1 on the background of an
430 estimated 75% seropositivity in Manaus Brazil (Faria et al., 2021). It seems possible that
431 selection of P.1 and B.1.351 may have been in part driven by immune escape, however until
432 methods are developed to screen at a population level for the frequency of reinfection, it is not
433 possible to determine this, especially as reinfection may lead to more mild or asymptomatic
434 disease.
435
436 Because P.1 and B.1.351 contain very similar changes in the RBD it might be assumed that
437 neutralization of both would be similarly affected. This was indeed the case for neutralization
438 by monoclonal antibodies directed at the RBD, where there was substantial escape from many
439 antibodies in our panel or from antibodies being developed for clinical use. However,
440 neutralization of P.1 was not compromised as severely as neutralization of B.1.351, when using
441 convalescent or vaccine serum induced by earlier SARS-CoV-2 strains(Zhou et al., 2021).
442 Using convalescent serum B.1.351 showed 13-fold reduction in neutralization compared to
443 Victoria whilst P.1 was only reduced 3.1-fold, comparable to the reduction seen with B.1.1.7,
444 which only harbours the single N501Y change in the RBD (Zhou et al., 2021;Supasa et al.,
445 2021). Similarly, neutralization of P.1 by vaccine serum was less impacted than neutralization
446 of B.1.351 meaning that vaccination with Wuhan S will likely provide some protection against
447 P.1. There is now clinical evidence that the ChAdOx1 nCoV-19 Oxford-AstraZeneca and
448 NVX-CoV2373 Novavax vaccines provide protection from B.1.1.7 (Emary et al.,
449 2021;Mahase, 2021). For B.1.351 both the Novavax
450 (https://www.webmd.com/vaccines/covid-19-vaccine/news/20210131/vaccine-not-as-
451 effective-against-south-african-variant) and Janssen vaccine
452 (https://www.reuters.com/article/us-health-coronavirus-vaccines-johnson-j-
453 idUSKBN29Z0F0) saw a marked decrease in efficacy against B.1.351, but still showed >50%

454 protection against moderate and severe disease, whilst in a Phase II trial, ChAdOx1 nCoV-19
455 efficacy against mild to moderate disease caused by B.1.351 was 10.4% (95% CI: –76.8; 43.8),
456 but efficacy against severe disease could not be assessed in this study (Madhi et al., 2021).
457
458 The reason for the differences in neutralization of B.1.351 and P.1 by immune serum are not
459 immediately clear, but presumably reflect the difference in the mutations introduced outside
460 the RBD. In addition to our mAb 159 a number of potent neutralizing mAbs have been reported
461 that map to the NTD (Cerutti et al., 2021), and this domain has multiple mutations in all three
462 major variant strains: B.1.1.7 has two deletions, B.1.351 has a deletion and four substitutions
463 and P.1 has 6 amino acid substitutions, including the creation of two N-linked glycan sequons
464 (**Figure 1 A-C**). Comparison of neutralization of pseudoviruses expressing only the three RBD
465 mutations (K417N E484K N501Y) of B.1.351 with pseudovirus expressing the full suite of
466 mutations in B.1.351 spike show that the non-RBD changes substantially increase escape from
467 neutralization (Wibmer et al., 2021;Dejnirattisai et al., 2021;Wang et al., 2021). The changes
468 in the NTD of the major variants are far less consistent than those found in the RBD, and there
469 are no strong trends in electrostatic properties (**Figure 1A-C**). It therefore remains unclear what
470 the drivers are for these changes, although one or more of immune escape, co-receptor binding,
471 and modulation of RBD dynamics affecting presentation of the receptor binding site are
472 plausible. Nonetheless, it seems likely that these changes are largely responsible for the non-
473 RBD component of neutralization variation between strains.
474
475 A number of public antibody responses have been reported for SARS-CoV-2, principal
476 amongst these being VH3-53/VH3-66 and VH1-58 (VH3-30 is also found but the antibodies
477 are not potent neutralizers) (Yuan et al., 2020;Barnes et al., 2020; Dejnirattisai et al., 2021).
478 We have previously shown that mixing heavy and light chains from antibodies within VH1-58

479 can increase the neutralization titre by 20-fold from the parent antibodies (chimera of 253HC
480 with 55LC or 165LC) (Dejnirattisai et al., 2021). Here we have shown that chimeras created
481 amongst the VH3-53 antibodies using the 222LC are able to confer broad neutralization to
482 antibodies which have reduced neutralization capacity against the viral variants. Furthermore,
483 the chimera of 150HC with 222LC achieved 13 and 3-fold increases in neutralization titre
484 compared to the parental 150 and 222 mAb respectively. Creation of such antibody chimeras
485 amongst other anti-SARS-CoV2 antibodies may similarly lead to the discovery of more
486 antibodies with enhanced activity. This also suggests that highly effective natural responses
487 against all three variants, and common cross-protective responses, will be found.
488
489 The recent emergence of a number of variants of concern has led to efforts to design new
490 vaccines which will be able to protect against the viral variants. Exactly which variants or
491 sequences should be selected is difficult to determine in what is likely to be an evolving
492 situation, as vaccine induced herd immunity increases the selection pressure for immune
493 escape. Based on the results reported here the South African B.1.351 is the variant of greatest
494 concern giving the largest reductions in neutralization titres and evidence of complete failure
495 to neutralize in some cases and we believe developing vaccine constructs to B.1.351 to be the
496 greatest priority.
497
498 In summary, we demonstrate that P.1 can escape neutralization by a number of monoclonal
499 antibodies including some being developed for prophylactic or therapeutic use, while other
500 antibodies with epitopes away from the mutated RBD residues retain broad neutralization.
501 Thus S309/AZD1061/REGN10987/ADG10/ADG20/ADG30 showed little to no reduction
502 (<4-fold) in neutralization activity across the three variants, consistent with their previously
503 described broadly neutralizing activities across clade I sarbecoviruses.

504

505 In contrast to B.1.351, neutralization of P.1 does not show such a substantial reduction by
506 polyclonal serum induced by natural infection or vaccination and there is no evidence of
507 widespread escape. Despite the reduction in neutralization titres it is hoped that immunization
508 with vaccines designed against parent/ancestral strains will provide protection from P.1.

509

510 **Limitations of the study**

511

512 The in vitro FRNT assays we report here do not measure the effect of complement or antibody
513 dependent cell mediated cytotoxicity which may enhance neutralization in vivo. The role that
514 T cells play in immunity to SARS-CoV-2 and in particular protection from severe disease is
515 unknown and worthy of investigation, but recent findings suggest that CD4 and CD8 T cell
516 responses raised to ancestral strains are minimally impacted by the variants (Alison Tarke et
517 al., 2021;Skelly et al., 2021). It will be interesting to determine the directionality of
518 neutralization between the different variant viruses and naturally acquired antibody responses
519 to them. For instance, there is some suggestion in this report that plasma induced by B.1.1.7 is
520 better able to neutralize B.1.351 and P.1. Measuring neutralization of viral variants by B.1.351
521 and P.1 serum will give a better idea of cross protection against the other strains.

522

523 **Acknowledgements**

524 This work was supported by the Chinese Academy of Medical Sciences (CAMS) Innovation
525 Fund for Medical Science (CIFMS), China (grant number: 2018-I2M-2-002) to D.I.S. and
526 G.R.S. H.M.E.D. and J.Ren are supported by the Wellcome Trust (101122/Z/13/Z), Y.Z. by
527 Cancer Research UK (C375/A17721), TAB and RJGH by the UKRI MRC (MR/S007555/1),
528 D.I.S. and E.E.F. by the UKRI MRC (MR/N00065X/1). D.I.S. is a Jenner Investigator. The

529 National Institute for Health Research Biomedical Research Centre Funding Scheme supports
530 G.R.S. We are also grateful for a Fast Grant from Fast Grants, Mercatus Center to support the
531 isolation of human monoclonal antibodies to SARS-CoV-2 and Schmidt Futures for support of
532 this work. G.R.S. is also supported as a Wellcome Trust Senior Investigator (grant
533 095541/A/11/Z). This is a contribution from the UK Instruct-ERIC Centre. The Wellcome
534 Centre for Human Genetics is supported by the Wellcome Trust (grant 090532/Z/09/Z). Virus
535 used for the neutralisation assays was isolated by Julian Druce, Doherty Centre, Melbourne,
536 Australia. Chanice Knight, Emily Chiplin, Ross Fothergill and Liz Penn contributed to assays.
537 We acknowledge Diamond Light Source for time on Beamline I03 under Proposal lb27009 for
538 COVID-19 Rapid Access. Huge thanks to the teams, especially at the Diamond Light Source
539 and Department of Structural Biology, Oxford University that have enabled work to continue
540 during the pandemic. The computational aspects of this research were supported by the
541 Wellcome Trust Core Award Grant Number 203141/Z/16/Z and the NIHR Oxford BRC. The
542 Oxford Vaccine work was supported by UK Research and Innovation, Coalition for Epidemic
543 Preparedness Innovations, National Institute for Health Research (NIHR), NIHR Oxford
544 Biomedical Research Centre, Thames Valley and South Midland's NIHR Clinical Research
545 Network. We thank the Oxford Protective T-cell Immunology for COVID-19 (OPTIC) Clinical
546 team for participant sample collection and the Oxford Immunology Network Covid-19
547 Response T cell Consortium for laboratory support. We acknowledge the rapid sharing of
548 Victoria, B.1.1.7 and B.1.351 which was isolated by scientists within the National Infection
549 Service at PHE Porton Down. We thank The Secretariat of National Surveillance, Ministry of
550 Health Brazil for assistance in obtaining P.1 samples. This work was supported by the UK
551 Department of Health and Social Care as part of the PITCH (Protective Immunity from T cells
552 to Covid-19 in Health workers) Consortium, the UK Coronavirus Immunology Consortium
553 (UK-CIC) and the Huo Family Foundation. EB and PK are NIHR Senior Investigators and PK

554 is funded by WT109965MA and NIH (U19 I082360). DS is an NIHR Academic Clinical
555 Fellow. The views expressed in this article are those of the authors and not necessarily those
556 of the National Health Service (NHS), the Department of Health and Social Care (DHSC), the
557 National Institutes for Health Research (NIHR), the Medical Research Council (MRC) or
558 Public Health, England.

559

560 **Author Information**

561 These authors contributed equally: WD, DZ, PS, CL, AJM.

562

563 **Contributions**

564 **Contributions**

565 D.Z. performed BLI interaction analyses. D.Z., J.R., N.G.P., M.A.W. and D.R.H. prepared the
566 crystals, enabled and performed X-ray data collection. J.R., E.E.F., H.M.E.D. and D.I.S.
567 analysed the structural results. G.R.S., J.M., P.S., Y.Z., D.Z., G.C.P, B.W., R.N., A.T., J.S-C.,
568 C.L-C. and C.L. prepared the Spike constructs, RBDs, ACE2 and antibodies and, W.D. and
569 P.S. performed neutralization assays. D.C. provided materials. H.M.G. wrote MABSCAPE and
570 performed mapping and cluster analysis, including sequence analyses. S.A.C.C., P. G. N.,
571 V.N., F. N., C. F. C., P.C.R., A.P-C., M.M.S., A.J.M., E.B., S.J.D., D.S., C.D., R.L., T.D.,
572 A.J.P., J.C.K., P.K., M.W.C., T.L., S.B., A.F., M.B., S.B-R., E.C. and S.G. assisted with patient
573 samples and vaccine trials. E.B., M.C., S.J.D., P.K. and D.S. conceived the study of vaccinated
574 healthcare workers and oversaw the OPTIC Healthcare Worker study and sample
575 collection/processing. G.R.S. and D.I.S. conceived the study and wrote the initial manuscript
576 draft with other authors providing editorial comments. R.J.G.H. and T.A.B. contributed to study
577 design. All authors read and approved the manuscript.

578

579 **Competing Financial Interests**

580 GRS sits on the GSK Vaccines Scientific Advisory Board. Oxford University holds intellectual
581 property related to the Oxford-AstraZeneca vaccine. AJP is Chair of UK Dept. Health and
582 Social Care's (DHSC) Joint Committee on Vaccination & Immunisation (JCVI) but does not
583 participate in the JCVI COVID19 committee, and is a member of the WHO's SAGE. The views
584 expressed in this article do not necessarily represent the views of DHSC, JCVI, or WHO. The
585 University of Oxford has entered into a partnership with AstraZeneca on coronavirus vaccine
586 development.
587 The University of Oxford has protected intellectual property disclosed in this publication.
588
589
590 **Figure Legends**
591
592 **Figure 1. Mutational landscape of P.1.** Schematic showing the locations of amino acid
593 substitutions in (A) P.1, (B) B.1.351 and (C) B.1.1.7 relative to the Wuhan SARS-CoV-2
594 sequence. Under the structural cartoon is a linear representation of S with changes marked on.
595 Where there is a charge change introduced by mutations the change is coloured (red if the
596 change makes the mutant more acidic/less basic, blue more basic/less acidic). (D) Depiction of
597 the RBD as a grey surface with the location of the three mutations K417T, E484K and N501Y
598 (magenta) the ACE2 binding surface of RBD is coloured green. (E) locations of N-linked
599 glycan (red spheres) on the spike trimer shown in a pale blue surface representation, the two
600 new sequons found in P.1 are marked blue.
601
602 **Figure 2. Comparison of WT RBD/ACE2 and P.1 RBD/ACE2 complexes.** (A)
603 Comparison of P.1 RBD/ACE2 (grey and salmon) with WT RBD/ACE2 (blue and cyan)

604 (PDB ID 6LZG) by overlapping the RBDs. The mutations in the P.1 RBD are shown as
605 sticks. (B), (C) Open book view of electrostatic surface of the WT RBD/ACE2 complex, and
606 (C), (D) of the P.1 RBD/ACE2 complex. Note the charge difference between the WT and the
607 mutant RBDs. The charge range displayed is ±5 kJ/mol. (E) The K417 of the WT RBD forms
608 a salt bridge with D30 of ACE2. (F) and (G) Effect of E484K mutation on the electrostatic
609 surface (H) Y501 of the P.1 RBD makes a stacking interaction with Y41 of ACE2. (H) K_D of
610 RBD/mAb interaction measured by BLI for RBDs of Victoria, B.1.1.7, P.1 and B.1.351 (left
611 to right) (I) BLI data mapped onto the RBD using the method described (Dejnirattisai *et al.*,
612 2021). Front and back views of the RBD are shown. In the left pair the spheres represent the
613 antibody binding sites coloured according to the ratio (K_DP.1/K_DWuhan). For white the ratio
614 is 1, for red it is <0.1 (i.e. at least 10-fold reduction) black dots refer to mapped antibodies
615 not included in this analysis, dark green RBD ACE2 binding surface, yellow mutated K417T,
616 E484K, N501Y. For the right pair atoms are coloured according to the ratio of neutralisation
617 titres (IC_{50}B.1.351/IC_{50}Victoria), for white the ratio is 1, for red it is <0.01 (i.e. at least 100-
618 fold reduction). Note the strong agreement between K_D and IC_{50}. 269 is very strongly
619 affected and is close to the IGHV3-53 and IGHV3-66 antibodies (*e.g.* 222).
620
621 **Figure 3. Neutralization of P.1 by monoclonal antibodies.** (A) Neutralization of P.1 by a
622 panel of 20 potent human monoclonal antibodies. Neutralization was measured by FRNT,
623 curves for P.1 are superimposed onto curves for Victoria, B.1.1.7 and B.1.351 as previously
624 reported (Supasa et al., 2021;Zhou et al., 2021). FRNT50 titres are reported in Table S2
625 Neutralization curves for monoclonal antibodies in different stages of development for
626 commercial use. (B) Shows equivalent plots for the Vir, Regeneron, AstraZeneca, Lilly and
627 Adagio antibodies therapeutic antibodies.
628

629 **Figure 4. Structures of Fab 222 in complex with P.1 RBD.** (A) Ribbon depiction of Fab
630 159/NTD complex with P1 mutations in the NTD highlighted as cyan spheres. (B) Front and
631 back surfaces of the RBD bound to a typical VH3-53. P1 mutations in the RBD are highlighted
632 in dark green and labelled. In this group, monoclonal antibody 222 has a slightly longer CDR3.
633 Sequences of VH3-53 CDR1-3 heavy and light chains are also shown. (C) Crystal structure of
634 P1 RBD, 222 Fab and EY6A Fab (Zhou et al., 2020). (D) Close up of 222 CDRs interacting
635 with the RBD (grey) mutations are highlighted in yellow on the green ACE2 interface. (E)
636 K417 interactions with Fab 222 (F) N501 interactions with Fab 222. (G), (H) Fab 222 chimera
637 models.
638
639 **Figure 5. Neutralization curves of VH3-53 chimeric antibodies.** Neutralization curves of
640 Victoria, B.1.1.7, B.1.351 and P.1. Left hand column; neutralization curves using the native
641 antibodies 222, 150, 158, 175 and 269. Right hand column; neutralization curves for chimeric
642 antibodies, the heavy chains of 150, 158, 175 and 269 are combined with the light chain of
643 222, native 222 is used as the control. FRNT50 titres are given in Table S2.
644
645 **Figure 6 Neutralization of P.1 by convalescent plasma.** Plasma (n=34) was collected from
646 volunteers 4-9 weeks following SARS-CoV-2 infection, all samples were collected before June
647 2020 and therefore represent infection before the emergence of B.1.1.7 in the UK. (A)
648 Neutralization of P.1 was measured by FRNT, comparison is made with neutralization curves
649 for Victoria, B.1.1.7 and B.1.351 that we have previously generated (Zhou et al., 2021;Supasa
650 et al., 2021). (B) Neutralization of P.1 by plasma taken from volunteers who had suffered
651 infection with B.1.1.7 as evidenced by sequencing or S-gene drop out by diagnostic PCR.
652 Samples were taken at varying times following infection. (C-D) Comparison of FRNT50 titres
653 between Victoria and P.1, data for B.1.1.7 and B.1.351 are included for comparison and, the

654 Wilcoxon matched-pairs signed rank test was used for the analysis and two-tailed P values
655 were calculated, geometric mean values are indicated above each column.
656
657 **Figure 7 Neutralization of P.1 by vaccine serum.** (A) Pfizer vaccine, serum (n=25) was taken
658 7-17 days following the second dose of the Pfizer-BioNTech vaccine. FRNT titration curves
659 are shown with Victoria, B.1.1.7 and B.1.351 as comparison (Supasa et al., 2021;Zhou et al.,
660 2021). (B) AstraZenca vaccine, serum was taken 14 or 28 days following the second dose of
661 the Oxford-AstraZeneca vaccine (n=25). (C-D) Comparison of FRNT50 titres for individual
662 samples for the Pfizer and AstraZeneca vaccine between Victoria, B.1.1.7, B.1.351 and P.1,
663 the Wilcoxon matched-pairs signed rank test was used for the analysis and two-tailed P values
664 were calculated, geometric mean values are indicated above each column.
665
666 **STAR Methods**
667 **RESOURCE AVAILABILITY**
668 *Lead Contact*
669 Resources, reagents and further information requirement should be forwarded to and will be
670 responded by the Lead Contact, David I Stuart (dave@strubi.ox.ac.uk).
671 *Materials Availability*
672 Reagents generated in this study are available from the Lead Contact with a completed
673 Materials Transfer Agreement.
674 *Data and Code Availability*
675 The coordinates and structure factors of the crystallographic complexes are available from the
676 PDB with accession codes (see Table S1). Mabscape is available from
677 https://github.com/helenginn/mabscape, https://snapcraft.io/mabscape. The data that support
678 the findings of this study are available from the corresponding authors on request.

679

680 **EXPERIMENTAL MODEL AND SUBJECT DETAILS**

681 *Viral stocks*

682 SARS-CoV-2/human/AUS/VIC01/2020 (Caly et al., 2020), SARS-CoV-2/B.1.1.7 and SARS-
683 CoV-2/B.1.351 were provided by Public Health England, P.1 from a throat swab from Brazil
684 were grown in Vero (ATCC CCL-81) cells. Cells were infected with the SARS-CoV-2 virus
685 using an MOI of 0.0001. Virus containing supernatant was harvested at 80% CPE and spun at
686 3000 rpm at 4 °C before storage at -80 °C. Viral titres were determined by a focus-forming
687 assay on Vero cells. Victoria passage 5, B.1.1.7 passage 2 and B.1.351 passage 4 stocks were
688 sequenced to verify that they contained the expected spike protein sequence and no changes to
689 the furin cleavage sites. The P.1 virus used in these studies contained the following mutations:
690 L18F, T20N, P26S, D138Y, R190S, K417T, E464K, N501Y, D614G, H655Y, T1027I,
691 V1176F. Passage 1 P.1 virus was sequence confirmed and contained no changes to the furin
692 cleavage site.

693 *Bacterial Strains and Cell Culture*

694 Vero (ATCC CCL-81) cells were cultured at 37 °C in Dulbecco's Modified Eagle medium
695 (DMEM) high glucose (Sigma-Aldrich) supplemented with 10% fetal bovine serum (FBS), 2
696 mM GlutaMAX (Gibco, 35050061) and 100 U/ml of penicillin–streptomycin. Human mAbs
697 were expressed in HEK293T cells cultured in UltraDOMA PF Protein-free Medium (Cat# 12-
698 727F, LONZA) at 37 °C with 5% CO_2. *E.coli DH5α* bacteria were used for transformation of
699 plasmids encoding wt and mutated RBD proteins. A single colony was picked and cultured in
700 LB broth with 50 µg mL^{-1} Kanamycin at 37 °C at 200 rpm in a shaker overnight. HEK293T
701 (ATCC CRL-11268) cells were cultured in DMEM high glucose (Sigma-Aldrich)
702 supplemented with 10% FBS, 1% 100X Mem Neaa (Gibco) and 1% 100X L-Glutamine

703 (Gibco) at 37 °C with 5% CO_2. To express RBD, RBD K417T, E484K, N501Y, RBD K417N,
704 RBD K417T, RBD E484K and ACE2, HEK293T cells were cultured in DMEM high glucose
705 (Sigma) supplemented with 2% FBS, 1% 100X Mem Neaa and 1% 100X L-Glutamine at 37
706 °C for transfection.

707 *Participants*

708 Participants were recruited through three studies: Sepsis Immunomics [Oxford REC C,
709 reference:19/SC/0296]), ISARIC/WHO Clinical Characterisation Protocol for Severe
710 Emerging Infections [Oxford REC C, reference 13/SC/0149] and the Gastro-intestinal illness
711 in Oxford: COVID sub study [Sheffield REC, reference: 16/YH/0247]. Diagnosis was
712 confirmed through reporting of symptoms consistent with COVID-19 and a test positive for
713 SARS-CoV-2 using reverse transcriptase polymerase chain reaction (RT-PCR) from an upper
714 respiratory tract (nose/throat) swab tested in accredited laboratories. A blood sample was taken
715 following consent at least 14 days after symptom onset. Clinical information including severity
716 of disease (mild, severe or critical infection according to recommendations from the World
717 Health Organisation) and times between symptom onset and sampling and age of participant
718 was captured for all individuals at the time of sampling.

719

720 P.1 virus from throat swabs. The International Reference Laboratory for Coronavirus at
721 FIOCRUZ (WHO) as part of the national surveillance for coronavirus had the approval of the
722 FIOCRUZ ethical committee (CEP 4.128.241) to continuously receive and analyze samples of
723 COVID-19 suspected cases for virological surveillance. Clinical samples (throat swabs)
724 containing P.1 were shared with Oxford University, UK under the MTA IOC FIOCRUZ 21-
725 02.

726

727

728 *Sera from Pfizer vaccinees*

729 Pfizer vaccine serum was obtained 7-17 days following the second dose of the BNT162b2
730 vaccine. Vaccinees were Health Care Workers, based at Oxford University Hospitals NHS
731 Foundation Trust, not known to have prior infection with SARS-CoV-2 and were enrolled in
732 the OPTIC Study as part of the Oxford Translational Gastrointestinal Unit GI Biobank Study
733 16/YH/0247 [research ethics committee (REC) at Yorkshire & The Humber – Sheffield]. The
734 study was conducted according to the principles of the Declaration of Helsinki (2008) and the
735 International Conference on Harmonization (ICH) Good Clinical Practice (GCP) guidelines.
736 Written informed consent was obtained for all patients enrolled in the study. Each received two
737 doses of COVID-19 mRNA Vaccine BNT162b2, 30 micrograms, administered
738 intramuscularly after dilution as a series of two doses (0.3 mL each) 18-28 days apart. The
739 mean age of vaccines was 43 years (range 25-63), 11 male and 14 female.

740

741 *AstraZeneca-Oxford vaccine study procedures and sample processing*

742 Full details of the randomized controlled trial of ChAdOx1 nCoV-19 (AZD1222), were
743 previously published (PMID: 33220855/PMID: 32702298). These studies were registered at
744 ISRCTN (15281137 and 89951424) and ClinicalTrials.gov (NCT04324606 and
745 NCT04400838). Written informed consent was obtained from all participants, and the trial is
746 being done in accordance with the principles of the Declaration of Helsinki and Good Clinical
747 Practice. The studies were sponsored by the University of Oxford (Oxford, UK) and approval
748 obtained from a national ethics committee (South Central Berkshire Research Ethics
749 Committee, reference 20/SC/0145 and 20/SC/0179) and a regulatory agency in the United
750 Kingdom (the Medicines and Healthcare Products Regulatory Agency). An independent
751 DSMB reviewed all interim safety reports. A copy of the protocols was included in previous
752 publications (PMID: 33220855/PMID: 32702298).

753

754 Data from vaccinated volunteers who received two vaccinations are included in this paper.
755 Vaccine doses were either 5×10^{10} viral particles (standard dose; SD/SD cohort n=21) or half
756 dose as their first dose (low dose) and a standard dose as their second dose (LD/SD cohort
757 n=4). The interval between first and second dose was in the range of 8-14 weeks. Blood
758 samples were collected and serum separated on the day of vaccination and on pre-specified
759 days after vaccination e.g. 14 and 28 days after boost.

760

761

762 **METHOD DETAILS**

763 *Focus Reduction Neutralization Assay (FRNT)*

764 The neutralization potential of Ab was measured using a Focus Reduction Neutralization Test
765 (FRNT), where the reduction in the number of the infected foci is compared to a negative
766 control well without antibody. Briefly, serially diluted Ab or plasma was mixed with SARS-
767 CoV-2 strain Victoria or P.1 and incubated for 1 hr at 37 °C. The mixtures were then transferred
768 to 96-well, cell culture-treated, flat-bottom microplates containing confluent Vero cell
769 monolayers in duplicate and incubated for a further 2 hrs followed by the addition of 1.5%
770 semi-solid carboxymethyl cellulose (CMC) overlay medium to each well to limit virus
771 diffusion. A focus forming assay was then performed by staining Vero cells with human anti-
772 NP mAb (mAb206) followed by peroxidase-conjugated goat anti-human IgG (A0170; Sigma).
773 Finally, the foci (infected cells) approximately 100 per well in the absence of antibodies, were
774 visualized by adding TrueBlue Peroxidase Substrate. Virus-infected cell foci were counted on
775 the classic AID EliSpot reader using **AID ELISpot software.** The percentage of focus
776 reduction was calculated and IC_{50} was determined using the probit program from the SPSS
777 package.

778

779 *Cloning of ACE2 and RBD proteins*

780 The constructs of EY6A Fab, 222 Fab, ACE2, WT RBD, B.1.1.7 and B.1.351 mutant RBD are
781 the same as previously described (Dejnirattisai et al. 2021, Zhou et al., 2021, Supasa et al.,
782 2021). To clone RBD K417T and RBD K417N, primers of RBD K417T (forward primer 5'-
783 GGGCAGACCGGCACGATCGCCGACTAC-3' and reverse primer 5'-
784 GTAGTCGGCGATCGTGCCGGTCTGCCC) and primers of RBD K417N (forward primer
785 5'-CAGGGCAGACCGGCAATATCGCCGACTACAATTAC-3' and reverse primer 5'-
786 GTAATTGTAGTCGGCGATATTGCCGGTCTGCCCTG-3') were used separately, together
787 with two primers of pNEO vector (Forward primer 5'- CAGCTCCTGGGCAACGTGCT-3'
788 and reverse primer 5'- CGTAAAAGGAGCAACATAG-3') to do PCR, with the plasmid of
789 WT RBD as the template. To clone P.1 RBD, the construct of B.1.351 RBD was used as the
790 template and the primers of RBD K417T and of pNEO vector mentioned above were used to
791 do PCR. Amplified DNA fragments were digested with restriction enzymes AgeI and KpnI
792 and then ligated with digested pNEO vector. All constructs were verified by sequencing.

793

794 *Protein production*

795 Protein production was as described in Zhou et al. (Zhou et al., 2020). Briefly, plasmids
796 encoding proteins were transiently expressed in HEK293T (ATCC CRL-11268) cells. The
797 conditioned medium was dialysed and purified with a 5-ml HisTrap nickel column (GE
798 Healthcare) and further polished using a Superdex 75 HiLoad 16/60 gel filtration column (GE
799 Healthcare).

800

801 *Bio-Layer Interferometry*

802 BLI experiments were run on an Octet Red 96e machine (Fortebio). To measure the binding
803 affinity of ACE2 with P.1 RBD and affinities of monoclonal antibodies and ACE2 with native
804 RBD and, RBD K417N, RBD K417T, RBD E484K and RBD K417T E484K N501Y, eachP.1
805 RBD, each RBD was immobilized onto an AR2G biosensor (Fortebio). Monoclonal antibodies
806 (Dejnirattisai et al., 2021) were used as analytes or serial dilutions of ACE2 were used as
807 analytes. All experiments were run at 30 °C. Data were recorded using software Data
808 Acquisition 11.1 (Fortebio) and Data Analysis HT 11.1 (Fortebio) with a 1:1 fitting model used
809 for the analysis.
810
811 *Antibody production*
812 AstraZeneca and Regeneron antibodies were provided by AstraZeneca, Vir, Lilly and Adagio
813 antibodies were provided by Adagio. For the chimeric antibodies heavy and light chains of the
814 indicated antibodies were transiently transfected into 293Y cells and antibody purified purified
815 from supernatant on protein A.
816
817 *Crystallization*
818
819 ACE2 was mixed with P.1 RBD in a 1:1 molar ratio to a final concentration of 12.5 mg ml^{-1}.
820 EY6A Fab, 222 Fab and WT or mutant RBD were mixed in a 1:1:1 molar ratio to a final
821 concentration of 7.0 mg ml^{-1}. All samples were incubated at room temperature for 30 min.
822 Most crystallization experiments was set up with a Cartesian Robot in Crystalquick 96-well X
823 plates (Greiner Bio-One) using the nanoliter sitting-drop vapor-diffusion method, with 100 nl
824 of protein plus 100 nl of reservoir in each drop, as previously described (Water et al., 2003).
825 Crystallization of B.1.1.7 RBD/EY6A/222 complex was set up by hand pipetting, with 500 nl
826 of protein plus 500 nl of reservoir in each drop. Good crystals of EY6A Fab and 222 Fab
827 complexed with WT, K417T, K417N, B.1.1.7, B.1.351 or P.1 RBD were all obtained from

828 Hampton Research PEGRx 2 screen, condition 35, containing 0.15 M Lithium sulfate, 0.1 M
829 Citric acid pH 3.5, 18% w/v PEG 6,000. Crystals of P.1 RBD/ACE2 complex were formed in
830 Hampton Research PEGRx 1 screen, condition 38, containing 0.1 M Imidazole pH 7.0 and
831 20% w/v Polyethylene glycol 6,000.
832
833 *X-ray data collection, structure determination and refinement*
834 Crystals of ternary complexes of WT and mutant RBD/EY6A and 222 Fabs and the P.1.
835 RBD/ACE2 were mounted in loops and dipped in solution containing 25% glycerol and 75%
836 mother liquor for a second before being frozen in liquid nitrogen prior to data collection.
837 Diffraction data were collected at 100 K at beamline I03 of Diamond Light Source, UK. All
838 data (except some of the WT RBD-EY6A-222 Fab complex images) were collected as part of
839 an automated queue system allowing unattended automated data collection
840 (https://www.diamond.ac.uk/Instruments/Mx/I03/I03-Manual/Unattended-Data-
841 Collections.html). Diffraction images of 0.1° rotation were recorded on an Eiger2 XE 16M
842 detector (exposure time of either 0.004 or 0.006 s per image, beam size 80×20 µm, 100% beam
843 transmission and wavelength of 0.9763 Å). Data were indexed, integrated and scaled with the
844 automated data processing program Xia2-dials (Winter, 2010;Winter *et al.*, 2018). A data set
845 of 1080° was collected from 3 positions of a frozen crystal for the WT RBD-EY6A-222 Fab
846 complex. 720° of data was collected for each of the B.1.1.7, P.1 and B.1.351 mutant
847 RBD/EY6A and 222 Fab complexes (each from 2 crystals), and 360° for each of the K417N
848 and K417T RBD with EY6A and 222 Fabs, and ACE2 complexes was collected from a single
849 crystal.
850
851 Structures of WT RBD-EY6A-222 and the P.1 RBD-ACE2 complexes were determined by
852 molecular replacement with PHASER (McCoy et al., 2007) using search models of SARS-

853 CoV-2 RBD-EY6A-H4 (PDB ID 6ZCZ) (Zhou et al., 2020) and RBD-158 (PDB ID, 7BEK)
854 (Dejnirattisai et al., 2021) complexes, and a RBD and ACE2 complex (PDB ID, 6LZG (Wang
855 et al., 2020)), respectively. Model rebuilding with COOT (Emsley and Cowtan, 2004) and
856 refinement with PHENIX (Liebschner et al., 2019) were done for all the structures. The ChCl
857 domains of EY6A are flexible and have poor electron density. Data collection and structure
858 refinement statistics are given in **Table S1**. Structural comparisons used SHP (Stuart et al.,
859 1979), residues forming the RBD/Fab interface were identified with PISA (Krissinel and
860 Henrick, 2007) and figures were prepared with PyMOL (The PyMOL Molecular Graphics
861 System, Version 1.2r3pre, Schrödinger, LLC).
862
863 *Quantification and statistical analysis*
864 Statistical analyses are reported in the results and figure legends. Neutralization was measured
865 by FRNT. The percentage of focus reduction was calculated and IC_{50} was determined using
866 the probit program from the SPSS package. The Wilcoxon matched-pairs signed rank test was
867 used for the analysis and two-tailed P values were calculated and geometric mean values. BLI
868 data were analysed using Data Analysis HT 11.1 (Fortebio) with a 1:1 fitting model.
869
870 References
871 Alison Tarke, A., Sidney, J., Methot, N., Zhang, Y., Dan, J.M., Goodwin, B., Rubiro, P.,
872 Sutherland, A., da Silva Antunes, R., Frazier, A., et al. Negligible impact of SARS-CoV-2
873 variants on CD4 + and CD8 + T cell reactivity in COVID-19 exposed donors and vaccinees.
874 *BioRxiv*. 2021; https://doi.org/10.1101/2021.02.27.433180.
875 Baden, L.R., El Sahly, H.M., Essink, B., Kotloff, K., Frey, S., Novak, R., Diemert, D., Spector,
876 S.A., Rouphael, N., Creech, C.B., et al. Efficacy and Safety of the mRNA-1273 SARS-CoV-2
877 Vaccine. *N. Engl. J. Med*. 2020; **384**: 403-416.

878 Barnes, C.O., West, A.P., Huey-Tubman, K.E., Hoffmann, M.A.G., Sharaf, N.G., Hoffman,
879 P.R., Koranda, N., Gristick, H.B., Gaebler, C., Muecksch, F., et al. Structures of Human
880 Antibodies Bound to SARS-CoV-2 Spike Reveal Common Epitopes and Recurrent Features
881 of Antibodies. *Cell* 2020; **182**: 828–842.
882 Baum, A., Fulton, B.O., Wloga, E., Copin, R., Pascal, K.E., Russo, V., Giordano, S., Lanza,
883 K., Negron, N., Ni, M., et al. Antibody cocktail to SARS-CoV-2 spike protein prevents rapid
884 mutational escape seen with individual antibodies. *Science*. 2020; ***369***: 1014–1018.
885 Caly, L., Druce, J., Roberts, J., Bond, K., Tran, T., Kostecki, R., Yoga, Y., Naughton, W.,
886 Taiaroa, G., Seemann, T., et al. Isolation and rapid sharing of the 2019 novel coronavirus
887 (SARS-CoV-2) from the first patient diagnosed with COVID-19 in Australia. *Med. J. Aust*.
888 2020; ***212***: 459–462.
889 Cerutti, G., Guo, Y., Zhou, T., Gorman, J., Lee, M., Rapp, M., Reddem, E.R., Yu, J., Bahna,
890 F., Bimela, J., et al.. Potent SARS-CoV-2 Neutralizing Antibodies Directed Against Spike N-
891 Terminal Domain Target a Single Supersite. *BioRxiv*. 2021: doi:
892 https://doi.org/10.1101/2021.01.10.426120
893 Dejnirattisai, W., Zhou, D., Ginn, H.M., Duyvesteyn, H.M.E., Supasa, P., Case, J.B., Zhao, Y.,
894 Walter, T.S., Mentzer, A.J., Liu, C., et al. The antigenic anatomy of SARS-CoV-2 receptor
895 binding domain. *Cell* 2021; doi: https://doi.org/10.1016/j.cell.2021.02.032
896 Domingo, E., and Perales, C. Viral quasispecies. *PLoS Genet.* 2019; **15:** e1008271.
897 https://doi.org/10.1371/journal.pgen.1008271
898 Donthu, N., and Gustafsson, A. Effects of COVID-19 on business and research. *J. Bus. Res*.
899 2020; **117**: 284–289.
900 Emary, K.R.W., Golubchik, T., Aley, P.K., Ariani, C. V., Angus, B.J., Bibi, S., Blane, B.,
901 Bonsall, D., Cicconi, P., Charlton, S., et al. Efficacy of ChAdOx1 nCoV-19 (AZD1222)

902 Vaccine Against SARS-CoV-2 VOC 202012/01 (B.1.1.7). *SSRN*. 2021; doi:
903 https://doi.org/10.2139/ssrn.3779160.
904 Emsley, P., and Cowtan, K. Coot: Model-building tools for molecular graphics. *Acta*
905 *Crystallogr. Sect. D Biol. Crystallogr.* 2004; **60**: 2126–2132.
906 Faria, N.R., Claro, I.M., Candido, D., Moyses Franco, L.A., Andrade, P.S., Coletti, T.M., Silva,
907 C.A.M., Sales, F.C., Manuli, E.R., Aguiar, R.S., et al. (2021). Genomic characterisation of an
908 emergent SARS-CoV-2 lineage in Manaus: preliminary findings - SARS-CoV-2 coronavirus /
909 nCoV-2019 Genomic Epidemiology - *Virological*, *virological.org*. Available at:
910 https://virological.org/t/genomic-characterisation-of-an-emergent-sars-cov-2-lineage-in-
911 manaus-preliminary-findings/586 (Accessed: 3 March 2021).
912 Greaney, A.J., Starr, T.N., Gilchuk, P., Zost, S.J., Binshtein, E., Loes, A.N., Hilton, S.K.,
913 Huddleston, J., Eguia, R., Crawford, K.H.D., et al. Complete Mapping of Mutations to the
914 SARS-CoV-2 Spike Receptor-Binding Domain that Escape Antibody Recognition. *Cell Host*
915 *Microbe.* 2021; **29**: 44-57.e9.
916 Hoffmann, M., Kleine-Weber, H., Schroeder, S., Mü, M.A., Drosten, C., and Pö, S. SARS-
917 CoV-2 Cell Entry Depends on ACE2 and TMPRSS2 and Is Blocked by a Clinically Proven
918 Protease Inhibitor. *Cell*. 2020; ***181***: 271-280.e8.
919 Kemp, S.A., Collier, D.A., Datir, R.P., Ferreira, I.A.T.M., Gayed, S., Jahun, A., Hosmillo, M.,
920 Rees-Spear, C., Mlcochova, P., Lumb, I.U., et al. SARS-CoV-2 evolution during treatment of
921 chronic infection. *Nature*. 2021; https://doi.org/10.1038/s41586-021-03291-y
922 Krammer, F. SARS-CoV-2 vaccines in development. *Nature*. 2020; **586**: 516–527.
923 Kreye, J., Reincke, S.M., Kornau, H.C., Sánchez-Sendin, E., Corman, V.M., Liu, H., Yuan,
924 M., Wu, N.C., Zhu, X., Lee, C.C.D., et al. A Therapeutic Non-self-reactive SARS-CoV-2
925 Antibody Protects from Lung Pathology in a COVID-19 Hamster Model. *Cell*. 2020; **183**:
926 1058–1069.

927 Krissinel, E., and Henrick, K. Inference of Macromolecular Assemblies from Crystalline State.
928 *J. Mol. Biol.* 2007; **372**: 774–797.
929 Ku, Z., Xie, X., Davidson, E., Ye, X., Su, H., Menachery, V.D., Li, Y., Yuan, Z., Zhang, X.,
930 Muruato, A.E., et al. Molecular determinants and mechanism for antibody cocktail preventing
931 SARS-CoV-2 escape. *Nat. Commun*. 2021; **12**: 469.
932 Liebschner, D., Afonine, P. V., Baker, M.L., Bunkoczi, G., Chen, V.B., Croll, T.I., Hintze, B.,
933 Hung, L.W., Jain, S., McCoy, A.J., et al. Macromolecular structure determination using X-
934 rays, neutrons and electrons: Recent developments in Phenix. *Acta Crystallogr. Sect. D Struct.*
935 *Biol.* 2019; **75**: 861–877.
936 Lu, R., Zhao, X., Li, J., Niu, P., Yang, B., Wu, H., Wang, W., Song, H., Huang, B., Zhu, N., et
937 al. Genomic characterisation and epidemiology of 2019 novel coronavirus: implications for
938 virus origins and receptor binding. *Lancet.* 2020; ***395***: 565–574.
939 Madhi, S.A., Baillie, V., Cutland, C.L., Voysey, M., Koen, A.L., Fairlie, L., Padayachee, S.D.,
940 Dheda, K., Barnabas, S.L., Bhorat, Q.E., et al. Safety and efficacy of the ChAdOx1 nCoV-19
941 (AZD1222) cOVID-19 vaccine against the B.1.351 variant in South Africa. *MedRxiv*. 2021;
942 doi: https://doi.org/10.1101/2021.02.10.21251247.
943 Mahase, E. (2021). Covid-19: Novavax vaccine efficacy is 86% against UK variant and 60%
944 against South African variant. *BMJ* 2021;372:n296
945 McCoy, A.J., Grosse-Kunstleve, R.W., Adams, P.D., Winn, M.D., Storoni, L.C., and Read,
946 R.J. Phaser crystallographic software. *J. Appl. Crystallogr. 2007;* ***40***: 658–674.
947 Pinto, D., Park, Y.J., Beltramello, M., Walls, A.C., Tortorici, M.A., Bianchi, S., Jaconi, S.,
948 Culap, K., Zatta, F., De Marco, A., et al. Cross-neutralization of SARS-CoV-2 by a human
949 monoclonal SARS-CoV antibody. *Nature* 2020; ***583***: 290–295.

950 Polack, F.P., Thomas, S.J., Kitchin, N., Absalon, J., Gurtman, A., Lockhart, S., Perez, J.L.,
951 Pérez Marc, G., Moreira, E.D., Zerbini, C., et al. Safety and Efficacy of the BNT162b2 mRNA
952 Covid-19 Vaccine. *N. Engl. J. Med*. 2020; **383**: 2603–2615.
953 Seemann, T., Lane, C.R., Sherry, N.L., Duchene, S., Gonçalves da Silva, A., Caly, L., Sait, M.,
954 Ballard, S.A., Horan, K., Schultz, M.B., et al. Tracking the COVID-19 pandemic in Australia
955 using genomics. *Nat. Commun*. 2020; **11**: 1–9.
956 Shang, J., Ye, G., Shi, K., Wan, Y., Luo, C., Aihara, H., Geng, Q., Auerbach, A., and Li, F.
957 Structural basis of receptor recognition by SARS-CoV-2. *Nature*. 2020; **581**: 221–224.
958 Skelly, D.T., Harding Sir William, A.C., Gilbert-Jaramillo Sir William, J., Knight Sir William,
959 M.L., Longet, S., Brown, A., Adele, S., Adland, E., Brown, H., and Stafford, L. (2021).
960 Vaccine-induced immunity provides more robust heterotypic immunity than natural infection
961 to emerging SARS-CoV-2 variants of concern. Research Square. 2021;
962 https://doi.org/10.21203/rs.3.rs-226857/v1.
963 Starr, T.N., Greaney, A.J., Dingens 1, A.S., and Bloom, J.D. (2021). Complete map of SARS-
964 CoV-2 RBD mutations that escape the monoclonal antibody LY-CoV555 and its cocktail with
965 LY-CoV016. B*ioRxiv*. 2021; https://doi.org/10.1101/2021.02.17.431683.
966 Stuart, D.I., Levine, M., Muirhead, H., and Stammers, D.K. Crystal structure of cat muscle
967 pyruvate kinase at a resolution of 2.6 Å. *J. Mol. Biol*. 1979; ***134*:** 109–142.Supasa, P., Zhou,
968 D., Dejnirattisai, W., Liu, C., Mentzer, A.J., Ginn, H.M., Zhao, Y., Duyvesteyn, H.M.E.,
969 Nutalai, R., Tuekprakhon, A., et al. (2021). Reduced neutralization of SARS-CoV-2 B.1.1.7
970 variant by convalescent and vaccine sera. *Cell*
971 2021;doi:https://doi.org/10.1016/j.cell.2021.02.033.
972 Tatusov, R.L., Galperin, M.Y., Natale, D.A., and Koonin, E. V. The COG database: A tool for
973 genome-scale analysis of protein functions and evolution. *Nucleic Acids Res*. 2000; **28:** 33–36.

974 Volz, E., Hill, V., McCrone, J.T., Price, A., Jorgensen, D., O'Toole, Á., Southgate, J., Johnson,
975 R., Jackson, B., Nascimento, F.F., et al. Evaluating the Effects of SARS-CoV-2 Spike Mutation
976 D614G on Transmissibility and Pathogenicity. *Cell*. 2021; ***184*:** 64-75.e11.
977 Voysey, M., Clemens, S.A.C., Madhi, S.A., Weckx, L.Y., Folegatti, P.M., Aley, P.K., Angus,
978 B., Baillie, V.L., Barnabas, S.L., Bhorat, Q.E., et al. Safety and efficacy of the ChAdOx1
979 nCoV-19 vaccine (AZD1222) against SARS-CoV-2: an interim analysis of four randomised
980 controlled trials in Brazil, South Africa, and the UK. *Lancet.* 2020; **397**: 99-111.
981 Walls, A.C., Park, Y.J., Tortorici, M.A., Wall, A., McGuire, A.T., and Veesler, D. Structure,
982 Function, and Antigenicity of the SARS-CoV-2 Spike Glycoprotein. *Cell*. 2020; **181**: 281-
983 292.e6.
984 Wang, P., Wang, M., Yu, J., Cerutti, G., Nair, M.S., Huang, Y., Kwong, P.D., Shapiro, L., *and*
985 *Ho, D.D.* Increased Resistance of SARS-CoV-2 Variant P.1 to Antibody Neutralization.
986 *bioRxiv* 2021; doi: https://doi.org/10.1101/2021.03.01.433466.
987 Wang, Q., Zhang, Y., Wu, L., Niu, S., Song, C., Zhang, Z., Lu, G., Qiao, C., Hu, Y., Yuen,
988 K.Y., et al. Structural and Functional Basis of SARS-CoV-2 Entry by Using Human ACE2.
989 *Cell*. 2020; **181**: 894-904.e9.
990 Wibmer, C.K., Ayres, F., Hermanus, T., Madzivhandila, M., Kgagudi, P., Oosthuysen, B.,
991 Lambson, B.E., de Oliveira, T., Vermeulen, M., van der Berg, K., et al. SARS-CoV-2 501Y.V2
992 escapes neutralization by South African COVID-19 donor plasma.
993 bioRxiv. 2021; doi: https://doi.org/10.1101/2021.01.18.427166
994 Winter, G. Xia2: An expert system for macromolecular crystallography data reduction. *J. Appl.*
995 *Crystallogr.* 2010; **43**: 186–190.
996 Winter, G., Waterman, D.G., Parkhurst, J.M., Brewster, A.S., Gildea, R.J., Gerstel, M.,
997 Fuentes-Montero, L., Vollmar, M., Michels-Clark, T., Young, I.D., et al. *DIALS*:

998 implementation and evaluation of a new integration package. *Acta Crystallogr. Sect. D Struct.*
999 *Biol*. 2018; **74**: 85–97.
1000 Wu, Y., Wang, F., Shen, C., Peng, W., Li, D., Zhao, C., Li, Z., Li, S., Bi, Y., Yang, Y., et al.
1001 A noncompeting pair of human neutralizing antibodies block COVID-19 virus binding to its
1002 receptor ACE2. *Science.* 2020; ***368***: 1274–1278.
1003 Yuan, M., Liu, H., Wu, N.C., Lee, C.C.D., Zhu, X., Zhao, F., Huang, D., Yu, W., Hua, Y.,
1004 Tien, H., et al. (2020). Structural basis of a shared antibody response to SARS-CoV-2. Science.
1005 2020; **369**: 1119–1123.
1006 Zahradník, J., Marciano, S., Shemesh, M., Zoler, E., Chiaravalli, J., Meyer, B., Dym, O., Elad,
1007 N., and Schreiber, G. SARS-CoV-2 RBD in vitro evolution follows contagious mutation
1008 spread, yet generates an able infection inhibitor. *BioRxiv*. 2021;
1009 https://doi.org/2021.01.06.425392.
1010 Zhou, D., Duyvesteyn, H.M.E., Chen, C.P., Huang, C.G., Chen, T.H., Shih, S.R., Lin, Y.C.,
1011 Cheng, C.Y., Cheng, S.H., Huang, Y.C., et al. Structural basis for the neutralization of SARS-
1012 CoV-2 by an antibody from a convalescent patient. *Nat. Struct. Mol. Biol*. 2020; **27**: 950–958.
1013 Zhou, D., Dejnirattisai, W., Supasa, P., Liu, C., Mentzer, A.J., Ginn, H.M., Zhao, Y.,
1014 Duyvesteyn, H.M.E., Tuekprakhon, A., Nutalai, R., et al. (2021). Evidence of escape of SARS-
1015 CoV-2 variant B.1.351 from natural and vaccine induced sera. *Cell*. 2021;
1016 https://doi.org/10.1016/j.cell.2021.02.037.
1017 Zost, S.J., Gilchuk, P., Case, J.B., Binshtein, E., Chen, R.E., Nkolola, J.P., Schäfer, A., Reidy,
1018 J.X., Trivette, A., Nargi, R.S., et al. Potently neutralizing and protective human antibodies
1019 against SARS-CoV-2. Nature 2020; **584**: 443–444.
1020

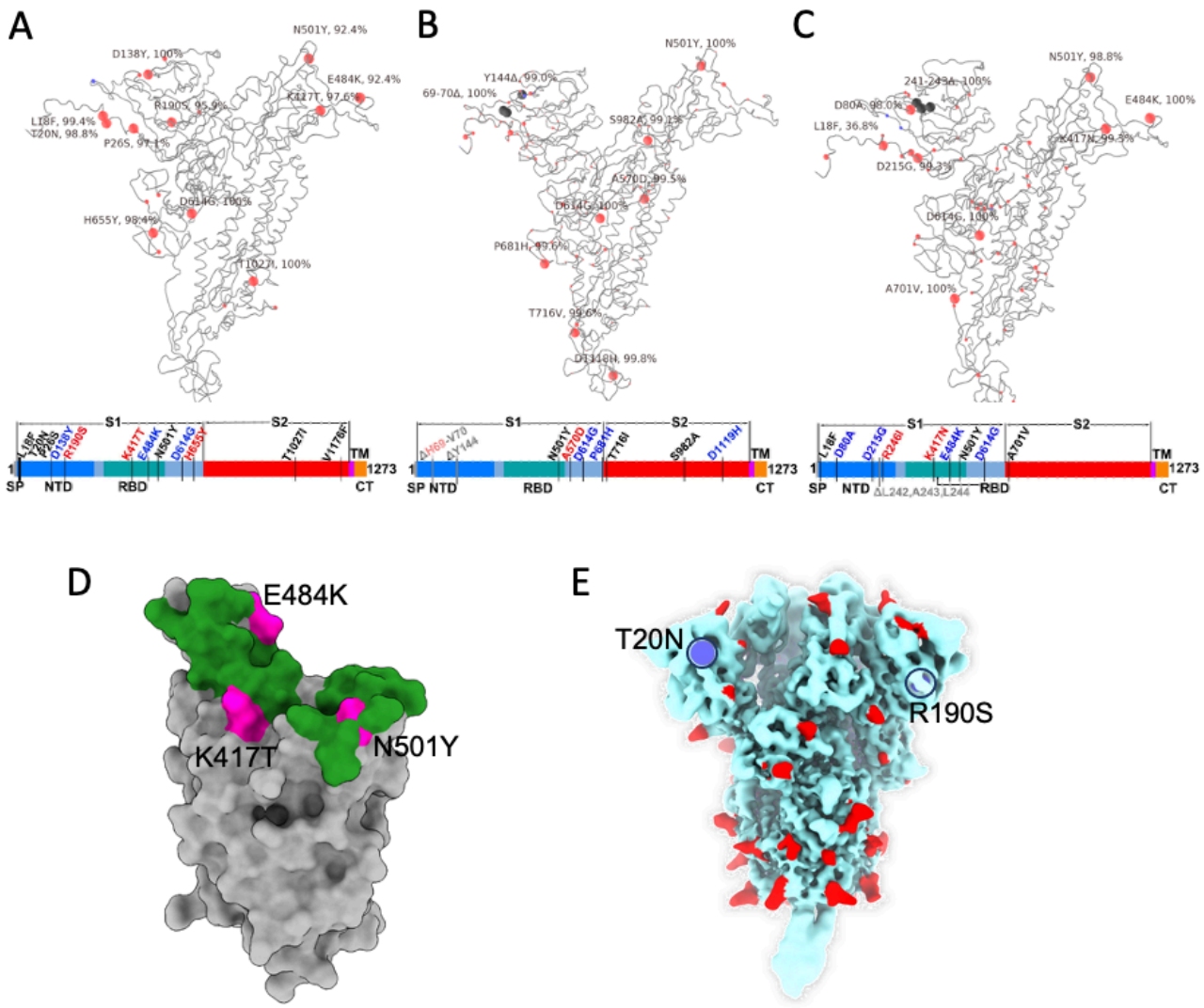
A
N501Y, 92.4%
D138Y, 100%
E484K, 92.4%
K417T, 97.6%
R190S, 95.9%
L18F, 99.4%
T20N, 98.8%
P26S, 97.1%
D614G, 100%
H655Y, 98.4%
T1027I, 100%
B
N501Y, 100%
Y144Δ, 99.0%
69-70Δ, 100%
S982A, 99.1%
A570D, 99.5%
D614G, 100%
P681H, 99.6%
T716V, 99.6%
D1118H, 99.8%
C
N501Y, 98.8%
241-243Δ, 100%
D80A, 98.0%
E484K, 100%
L18F, 36.8%
K417N, 99.3%
D215G, 99.3%
D614G, 100%
A701V, 100%
S1
S2
SP
NTD
RBD
CT
TM
1
1273
D
E484K
K417T
N501Y
E
T20N
R190S

Figure1

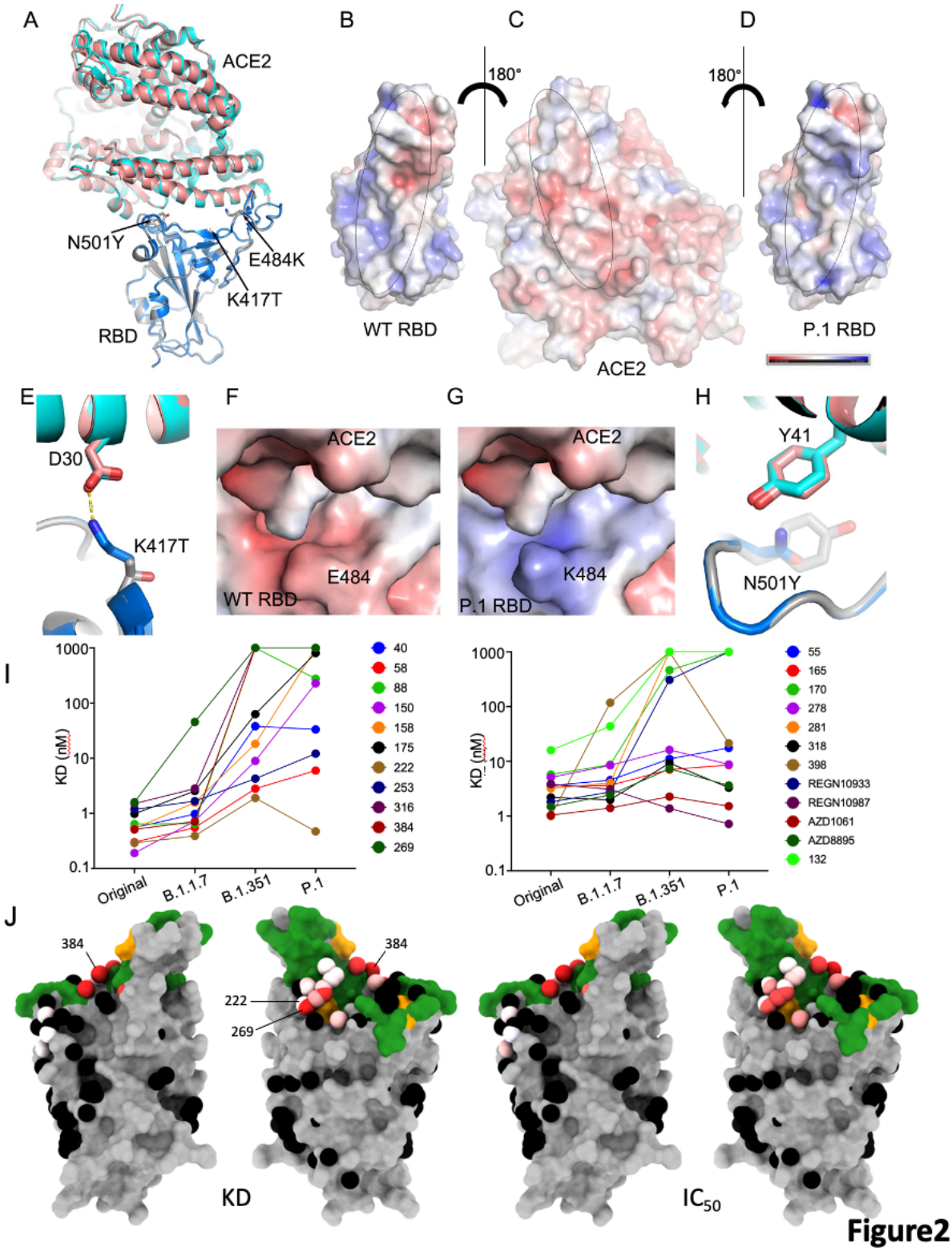
A
ACE2
N501Y
E484K
K417T
RBD
B
C
D
180°
180°
WT RBD
ACE2
P.1 RBD
E
D30
K417T
F
ACE2
E484
WT RBD
G
ACE2
K484
P.1 RBD
H
Y41
N501Y
I
KD (nM)
1000
100
10
1
0.1
Original
B.1.1.7
B.1.351
P.1
40
58
88
150
158
175
222
253
316
384
269
55
165
170
278
281
318
398
REGN10933
REGN10987
AZD1061
AZD8895
132
J
384
222
269
KD
IC50

Figure2

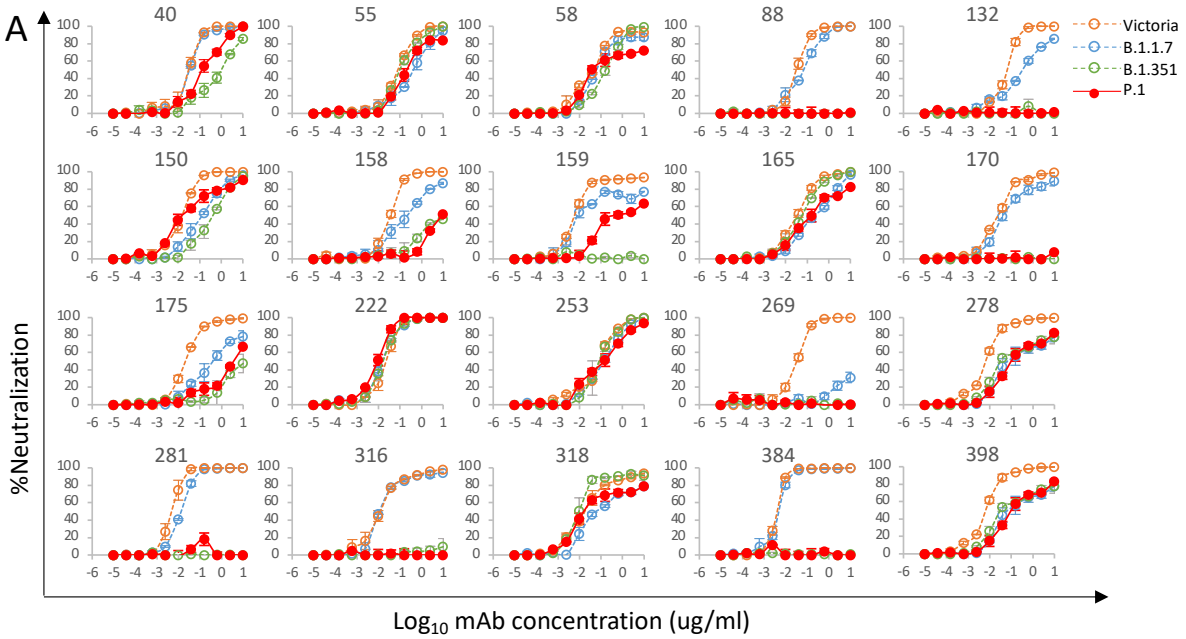

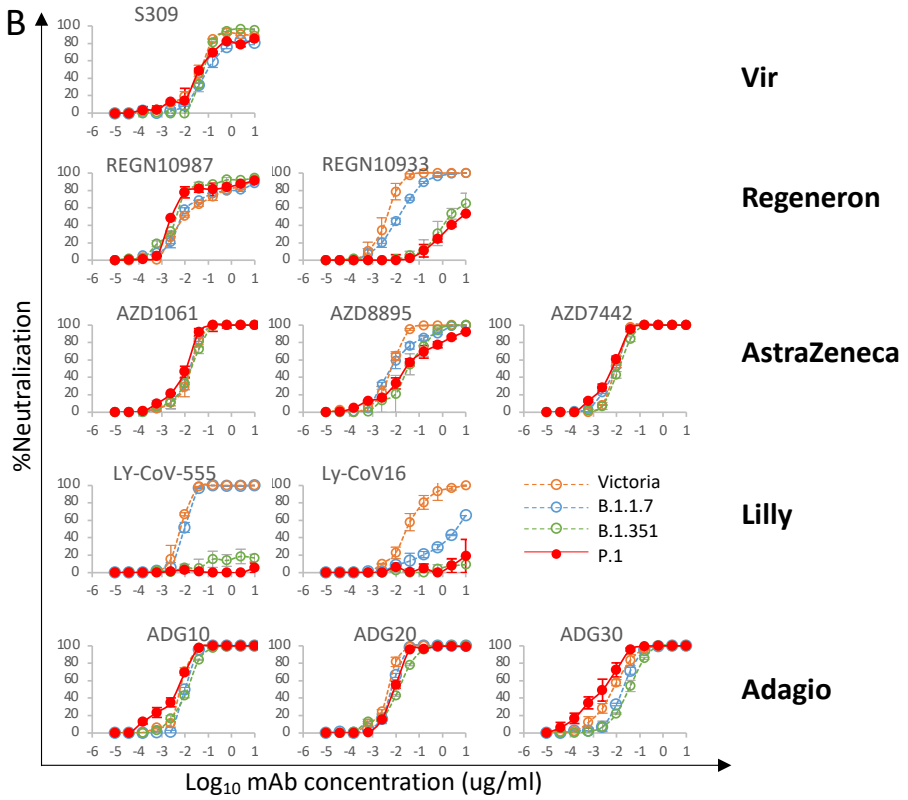

Figure3

1025

1026

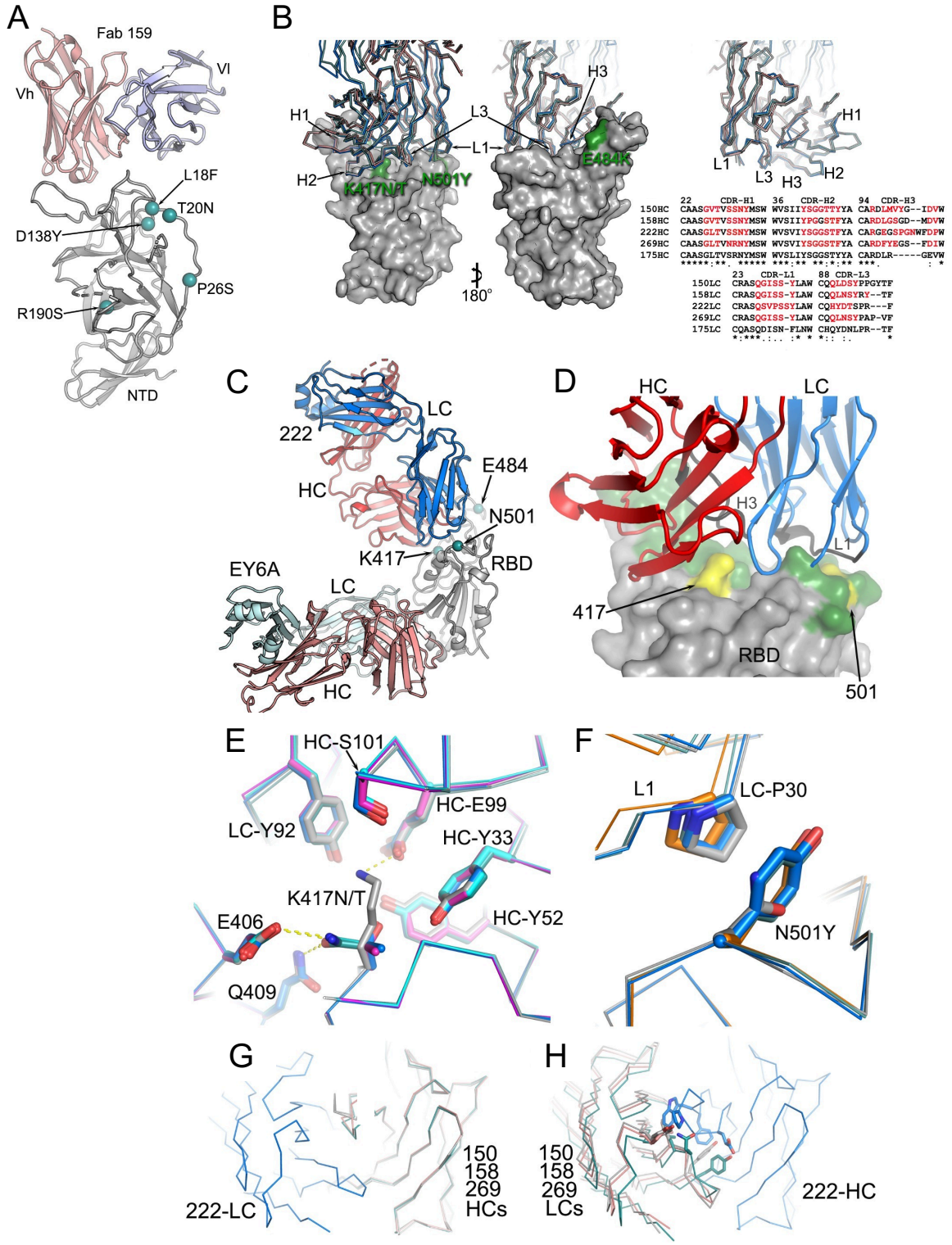

Figure4

1027

1028

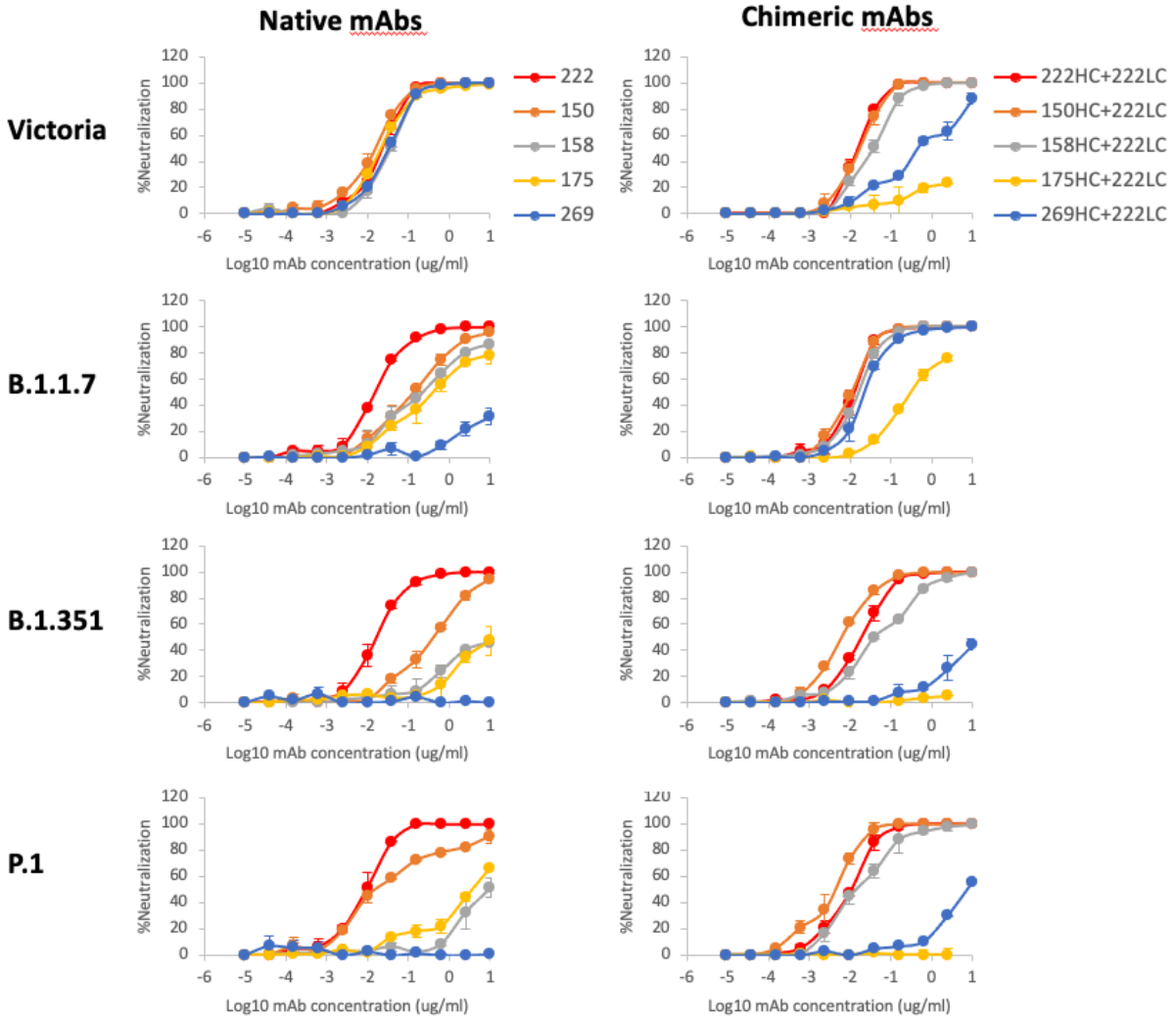

1029

1030

Figure5

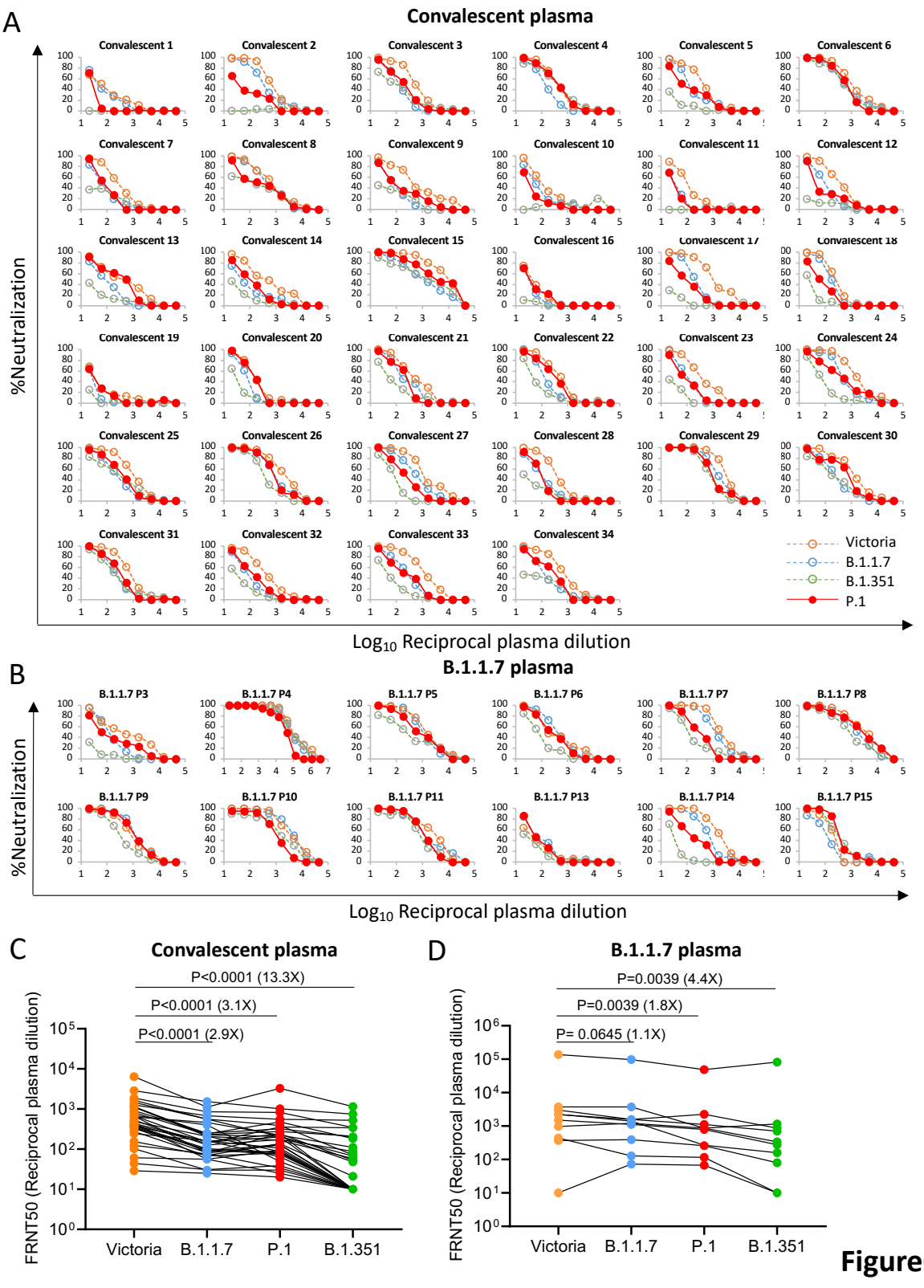
A
Convalescent plasma
%Neutralization
Log10 Reciprocal plasma dilution
Victoria
B.1.1.7
B.1.351
P.1
B
B.1.1.7 plasma
%Neutralization
Log10 Reciprocal plasma dilution
C
Convalescent plasma
P<0.0001 (13.3X)
P<0.0001 (3.1X)
P<0.0001 (2.9X)
FRNT50 (Reciprocal plasma dilution)
Victoria
B.1.1.7
P.1
B.1.351
D
B.1.1.7 plasma
P=0.0039 (4.4X)
P=0.0039 (1.8X)
P= 0.0645 (1.1X)
FRNT50 (Reciprocal plasma dilution)
Victoria
B.1.1.7
P.1
B.1.351

Figure6

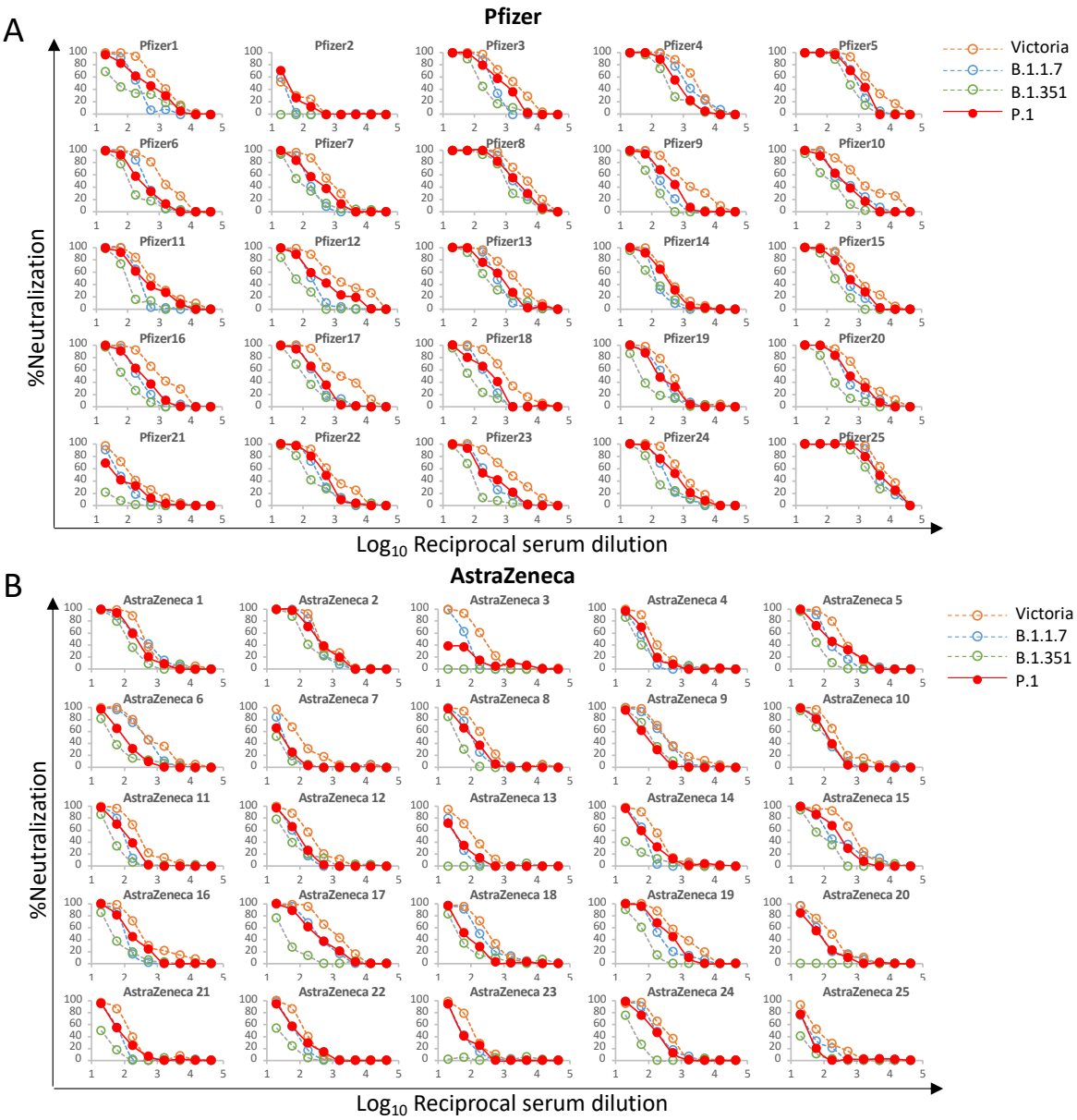

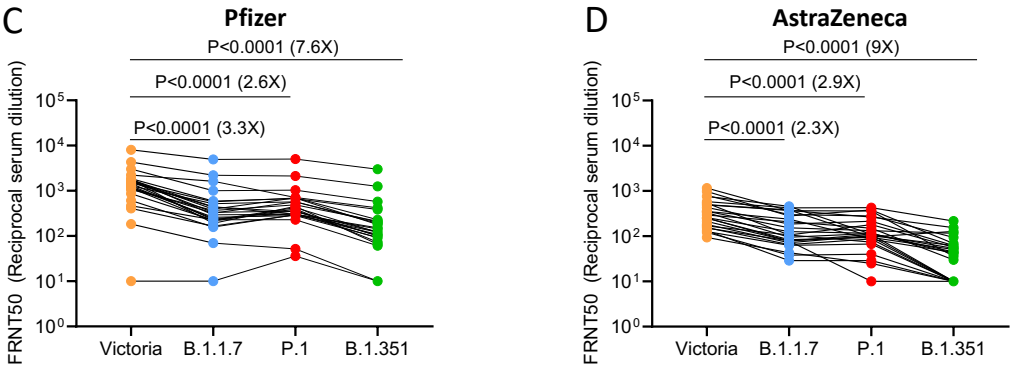

Figure7

1033